Received: 29 November 2021 | Revised: 4 March 2022 | Accepted: 7 March 2022

DOI: 10.1002/nme.6969

RESEARCH ARTICLE

WILEY

Crystal plasticity algorithm based on the quasi-extremal energy principle

Henryk Petryk | **Michal Kursa**

Institute of Fundamental Technological Research, Polish Academy of Sciences, Warsaw, Poland

Correspondence
Henryk Petryk, Institute of Fundamental Technological Research, Polish Academy of Sciences, Pawinskiego 5B, 02-106 Warsaw, Poland.
Email: hpetryk@ippt.pan.pl

Abstract

The direct incremental energy minimization in rate-independent plasticity does not account for the skew-symmetric part of the tangent stiffness matrix. In crystal plasticity, this corresponds to neglecting the asymmetry of the matrix of interaction moduli for active slip-systems. This limitation has been overcome in the recently proposed quasi-extremal energy principle (QEP) applicable to nonpotential problems. In the present article it is shown how to extend QEP to finite increments in the backward-Euler computational scheme. A related constitutive algorithm is proposed which enables automatic selection of active slip systems using an energetic criterion, along any path of large deformation of a rate-independent single crystal with a nonsymmetric slip-system interaction matrix. Numerical examples have been calculated for a fcc single crystal subjected to simple shear or uniaxial tension. The slip system activity predicted by using the QEP algorithm has been found to be more reliable in describing the actual plastic response of metal crystals than conventional rate-dependent modeling in cases where the selection of active slip-systems is essential.

KEYWORDS

solids, plasticity, material stability, Lagrangian, slip-system selection, time integration, implicit

1 | INTRODUCTION

In this article, an energy-based constitutive algorithm for the rate-independent crystal plasticity is developed which enables automatic selection of active slip systems along any paths of large deformation. The algorithm generates the values of incremental slips which, in the limit of a vanishingly small time step, provide an exact solution to the constitutive rate-problem. In contrast to the previous energy-based algorithms, there is no restriction here on the symmetry of the slip-system interaction matrix. However, this required a more fundamental extension of the incremental energy minimization approach, applicable to potential problems, to a broader concept of incremental *quasi-minimization* of energy.[1]

There are commonly known branching phenomena like buckling, necking, shear banding or subgrain formation which in numerical simulations require a criterion of choice of the postcritical deformation branch. In the rate-independent crystal plasticity at finite strain, the problem of nonuniqueness appears already at the constitutive level of selection of active slip systems at a material point.[2-4] General conditions sufficient and necessary for uniqueness of the solution for slip-rates in the rate-independent framework[2,5] are not satisfied in general. If there exists an incremental potential then a computational approach based on the incremental energy minimization is available for selecting the slip-system set of physical meaning.[6,7] However, a generic rate-problem in crystal plasticity is of nonpotential type due

to the lack of symmetry of the slip-system interaction matrix.[3,4] Therefore, the question arises how to select a physically meaningful solution among multiple possibilities when the known extremal principles do not apply.

Recently, a new energy-based variational formulation has been developed for a broad class of nonpotential problems in rate-independent plasticity.[1] It has been demonstrated that the direct incremental energy minimization does not provide a proper solution to the rate-problem posed if the global stiffness matrix for active plastic deformation mechanisms is not symmetric. A correct rate-solution is then generated by a *quasi-extremal energy principle* (QEP) in which the minimized function depends on an unknown solution as a parameter. When specialized in the constitutive rate-problem of rate-independent plasticity, this reduces to the quasi-minimization of the incremental energy expression that consists of the standard quadratic expression for deformation work and a new bilinear form based on the *skew* part of the slip-system interaction matrix.

The aim of this article is twofold. First, to extend the quasi-extremal energy principle, formulated originally in Reference 1 for rate-solutions to nonpotential problems, to small but finite increments with end-point values as unknowns in the computational approach. Second, to apply the principle in numerical simulations of large plastic deformations of a single crystal to automatically select currently active slip systems at each time step, without assuming symmetry of the slip-system interaction matrix.

While the quasi-extremal principle formulated in Reference 1 encompasses the gradient-enhanced plasticity, the algorithmic problem examined in this article is local, that is, formulated in the continuum mechanics framework at a single material point without slip-gradient effects. The classical constitutive theory of elastic-plastic crystals deformed by multislip at large strain has been established by Hill and Rice,[2,8,9] later reformulated and used in many works, for example, References 3,10-12 and others. Although it is not necessary in this article, for the sake of simplicity we adopt the generalized Schmid (normality) rule, the meaning of which has been thoroughly discussed in Reference 2. Nonassociative plasticity (cf. Reference 13) is included in the variational formulations recently proposed in References 1 and 14 for rate-independent thermodynamic systems. Variational formulations and slip-system selection in the gradient-enhanced crystal plasticity represent another topic, see References 15-22, which is not addressed here.

An overview of different algorithmic approaches to rate-independent crystal-plasticity was presented in Reference 23. Earlier algorithms for multisurface plasticity[24,25] are of limited applicability as the slip-systems interaction matrix, $(g^{\alpha\beta})$, need not satisfy any of the standard conditions of (i) linear independence of systems, (ii) positive definiteness, and (iii) symmetry. An iterative procedure for selecting active slip-systems in crystal plasticity in the geometrically linear setting was developed in Reference 26 and in the finite-strain framework in References 27 and 28. In outline, it proceeds by eliminating slip-systems which correspond to negative slips and adding overloaded slip-systems which correspond to positive values of the yield functions. Another algorithm based on an augmented Lagrangian formulation of the principle of maximum plastic dissipation was proposed in Reference 29. In turn, if the set of active slip-systems is prescribed, the incremental slips are determined by solving a system of (linear or nonlinear) equations. When the active slip-systems are linearly dependent then this can lead to a singular or ill-conditioned problem. In such cases, the pseudo-inverse or generalized inverse methods can be used.[27,28,30] Subsequently, other algorithms have been developed, compare References 31-37 and the references therein. The closest to the present article are the works based on the incremental energy minimization,[6,7,21,38-47] but they require existence of an incremental potential, which is a separate assumption in the general case.

In all these studies, however, the following significant question remained open: how to proceed in the rate-independent crystal plasticity if there are nonunique incremental solutions associated with *distinct* sets of active slip-systems in a generic *nonpotential* case. This work aims to fill that gap.

The nonuniqueness problem in crystal plasticity is often circumvented by applying a rate-dependent (viscoplastic) model in which the slip-rates are uniquely defined in a given state, see References 9,35,37,48-53 and many other works. This clear advantage is, however, accompanied by the difficulties related to a "stiff" system of highly nonlinear equations obtained for low rate-sensitivity, which is typical for metals at room temperature and usually requires the use of a small time step in the calculations. The lack of nonuniqueness in crystal viscoplasticity may also be accompanied by strong sensitivity of a solution to initial imperfections, for example, to the alignment of crystallographic axes to the loading axis,[49] or exponential growth of perturbations.[53] It is an open question whether the variational formulation of viscoplastic constitutive updates based on minimization of a quasi-thermodynamic function treated as constitutive potential, for example References 54-57, can be used to deal with the issue of imperfection sensitivity. By simply solving the set of incremental constitutive equations in a high-symmetry orientation of the crystal while maintaining the geometric symmetry, either within the rate-dependent or rate-independent framework, the predicted number of active slip systems can be excessive in comparison with experiments, which is illustrated in Section 5.2 below.

The article is organized as follows. Sections 2.1–2.4 provide the needed mathematical background for the quasi-extremal energy principle (QEP) in its formulation for the constitutive rate problem of rate-independent crystal plasticity with an arbitrary (nonsymmetric) slip-system interaction matrix. Coefficients of the constitutive rate equations are given a more specific form in Section 2.5 within the conventional crystal plasticity framework at finite deformation. In Section 3 and Appendix, the extension of QEP to the case of finite increments is derived. It is used in the computational algorithm described in detail in Section 4 and given in Boxes 1–4 in the form ready for implementation. Applicability of the algorithm to slip-system selection is demonstrated in Section 5 through numerical simulations of large deformation of a fcc single crystal under simple shear and uniaxial tension, with comparison to the results generated by other algorithms. Basic conclusions are summarized in Section 6.

2 | CONSTITUTIVE FRAMEWORK AND MATHEMATICAL BACKGROUND

2.1 | The rate-independent framework for crystal plasticity

Due to inherent path dependence of the response of an elastic-plastic material to the applied loads or displacements, the basic problem to be solved is formulated in a time-continuous setting in the rate form. This article is limited to the description of the quasi-static isothermal behavior of ductile single crystals.

In the finite deformation framework, the quasi-static rate problem of continuing equilibrium takes the simplest form in terms of the rate $\dot{\mathbf{S}}$ of the Piola stress $\mathbf{S}$ (the first Piola–Kirchhoff stress tensor). For typical boundary conditions in the assumed absence of body forces, the problem of continuing equilibrium is formulated in the standard notation as follows*

$$\mathrm{Div}\,\dot{\mathbf{S}} = \mathbf{0} \quad \text{in } \mathcal{B}, \qquad \dot{\mathbf{u}} = \overline{\mathbf{v}} \quad \text{on } \partial\mathcal{B}_{\mathrm{u}}, \qquad \dot{\mathbf{S}}\mathbf{n} = \dot{\mathbf{T}} \quad \text{on } \partial\mathcal{B}_{\mathrm{T}}. \tag{1}$$

Here, $\mathcal{B}$ is a domain occupied by a material body in a fixed reference configuration, on a part $\partial\mathcal{B}_{\mathrm{u}}$ of the body boundary $\partial\mathcal{B}$ a velocity $\dot{\mathbf{u}}$ takes a prescribed value $\overline{\mathbf{v}}$, while on the complementary part $\partial\mathcal{B}_{\mathrm{T}} = \partial\mathcal{B} \setminus \partial\mathcal{B}_{\mathrm{u}}$ of unit outward normal $\mathbf{n}$ the nominal traction rate $\dot{\mathbf{T}}$ is prescribed. If, at a material point, $\dot{\mathbf{S}}$ is a known function of velocity gradient then the velocity field is the basic unknown in problem (1).

In crystal plasticity, or more generally in case of multiple inelastic deformation mechanisms of rate-independent type, at a material point there are other basic unknowns, commonly known as slip-rates or plastic multipliers, denoted here as $\dot{\gamma}^\alpha$, $\alpha = 1, \ldots, N$. A Greek superscript α is used throughout as an index of the crystallographic slip-system (and not an exponent). Each plastic multiplier $\dot{\gamma}^\alpha$ is related to f^α, the value of a corresponding yield function for the αth slip-system, to be defined later. The respective vectors are denoted by $(\dot{\gamma}^\alpha) \in \mathbb{R}^N$ and $(f^\alpha) \in \mathbb{R}^N$.

Generic constitutive rate-equations of crystal plasticity at finite strain were originally formulated in an objective form by Hill and Rice.[2] By using the known transformation rules,[5,58] they can be expressed in the Lagrangian formulation as follows

$$\dot{\mathbf{S}} = \mathbb{C}^{\mathrm{e}} \cdot \dot{\mathbf{F}} - \sum_{\alpha\in\mathcal{N}} \mathbf{\Lambda}^\alpha_{\mathrm{p}} \dot{\gamma}^\alpha, \qquad \dot{f}^\alpha = \dot{\mathbf{F}} \cdot \mathbf{\Lambda}^\alpha - \sum_{\beta\in\mathcal{N}} g^{\alpha\beta}\dot{\gamma}^\beta \qquad \text{for } \alpha \in \mathcal{N} = \{1, \ldots, N\}. \tag{2}$$

Here, $\mathbb{C}^{\mathrm{e}} = \overset{\mathrm{T}}{\mathbb{C}}{}^{\mathrm{e}}$ is the fourth-order elastic stiffness tensor that provides the link between $\dot{\mathbf{S}}$ and $\dot{\mathbf{F}} = \nabla\dot{\mathbf{u}}$, the rate of deformation gradient equal to the velocity gradient in a fixed reference configuration, the sum of $\mathbf{\Lambda}^\alpha_{\mathrm{p}}\dot{\gamma}^\alpha$ defines the direction of plastic stress-rate $\dot{\mathbf{S}}^{\mathrm{p}} = \dot{\mathbf{S}} - \mathbb{C}^{\mathrm{e}} \cdot \nabla\dot{\mathbf{u}}$, and $\mathbf{\Lambda}^\alpha$ is the αth yield-surface normal transformed to $\mathbb{R}^{3\times3}$ space. The quantities $\mathbb{C}^{\mathrm{e}}, \mathbf{\Lambda}^\alpha_{\mathrm{p}}, \mathbf{\Lambda}^\alpha, g^{\alpha\beta}$ are all dependent on the current state of the material, denoted by $\mathcal{G}$, in a manner which will be specified in Section 2.5, and represent coefficients of the otherwise *linear* rate-equations (2).

After suitable normalization which is assumed, $\mathbf{\Lambda}^\alpha_{\mathrm{p}} = \mathbf{\Lambda}^\alpha$ corresponds to the normality flow rule for the αth slip system (see References 2,7,10 for more details), and $\mathbf{\Lambda}^\alpha_{\mathrm{p}} \nparallel \mathbf{\Lambda}^\alpha$ to a nonassociative flow rule for the plastic slip with non-Schmid effects.[12,59] Throughout this article, we restrict attention to the normality flow rule, $\mathbf{\Lambda}^\alpha_{\mathrm{p}} = \mathbf{\Lambda}^\alpha$. The (measure-invariant) slip-system interaction matrix $(g^{\alpha\beta})$ includes strain hardening/softening dominated by a quadratic form based on the elastic stiffness tensor, see References 2 and 10 and Section 2.5 for details. The state-dependent matrix $(g^{\alpha\beta})$ will play an essential role in what follows.

The basic rule of plastic slip-system activity in the rate-independent framework is assumed in the well-known form

$$\dot{\gamma}^\alpha \geq 0, \quad f^\alpha \leq 0, \quad f^\alpha \dot{\gamma}^\alpha = 0 \qquad \text{for } \alpha \in \mathcal{N}. \tag{3}$$

Nonzero values of $\dot{\gamma}^\alpha$'s cannot be uniquely determined from rule (3) applied in a given state $\mathcal{G}$ at a single instant only, see Section 2.2. An unknown slip-rate $\dot{\gamma}^\alpha$ in the plastic region where $f^\alpha = 0$ must additionally satisfy the consistency conditions

$$\dot{f}^\alpha \leq 0, \qquad \dot{f}^\alpha \dot{\gamma}^\alpha = 0 \qquad \text{if } f^\alpha = 0, \tag{4}$$

which makes the constitutive rate-problem inherently nonlinear (actually piecewise-linear).

The entire rate-problem to be solved is defined by Equations (1), (2), (3), and (4). In this article, the basic constitutive rate-problem of rate-independent crystal plasticity is isolated for study as follows.

Constitutive Rate-Problem. In a given state $\mathcal{G}$ and for prescribed $\dot{\mathbf{F}}$, find $\dot{\gamma}^\alpha$ that satisfy the conditions $(2)_2, (3)$ and (4) for all $\alpha \in \mathcal{N}$ simultaneously. (5)

If the Constitutive Rate-Problem has been solved at each spatial integration point then Equation (1) reduces to a nonlinear problem for a velocity field $\dot{\underline{\mathbf{u}}}$.

2.2 | Minimum principle for the first-order work

A variational formulation of the slip-system activity rule (3) is frequently obtained, following,[60,61] from the principle of maximum plastic work or maximum dissipation rate, the maximum reached among admissible *stresses*. It is well known that this implies the normality flow rule relative to a nonempty elastic domain.

However, without these limitations, the activity rule (3) for a slip-rate solution $(\dot{\gamma}^\alpha)$ can be given an *equivalent* variational form by referring to the minimum principle for a *virtual work-rate* $\tilde{w}$ (per unit reference volume), treated as a function of virtual *slip-rates*. The virtual work-rate, when expressed as a sum of virtual rates of the free energy and dissipation densities, takes the form given in References 7 and 62

$$\tilde{w} = \mathbf{S} \cdot \tilde{\mathbf{F}} - \sum_{\alpha \in \mathcal{N}} f^\alpha \tilde{\gamma}^\alpha. \tag{6}$$

Henceforth, a superimposed tilde denotes a *virtual* rate which needs to be distinguished from the *actual* rate denoted by a superimposed dot. A nonzero last term in the expression for $\tilde{w}$ for a *virtual* slip-rate $\tilde{\gamma}^\alpha$ can be interpreted as a result of perturbation imposed by a disturbing agency on the actual internal forces.[62] To examine the local constitutive problem posed in a given material state $\mathcal{G}$ for a prescribed $\dot{\mathbf{F}}$, we restrict attention to $\tilde{\mathbf{F}} = \dot{\mathbf{F}}$, so that $\tilde{w}$ becomes a linear function of $\tilde{\gamma}^\alpha$ only.

The following simple lemma provides the basic variational formulation of the slip-system activity rule (3).

Lemma 1. *In a given state $\mathcal{G}$, where $(\mathbf{S}, f^\alpha)$ are known, the following two statements are equivalent:*

(i) *$(\dot{\gamma}^\alpha)$ satisfies the slip-system activity rule (3),*
(ii) *$(\dot{\gamma}^\alpha)$ satisfies the minimum work-rate principle*

$$\dot{w}(\dot{\gamma}^\alpha) \leq \tilde{w}(\tilde{\gamma}^\alpha) \qquad \forall \tilde{\gamma}^\alpha \geq 0 \qquad \text{for given } \tilde{\mathbf{F}} = \dot{\mathbf{F}}. \tag{7}$$

Proof. It follows immediately from the mathematical theorem on the necessity and sufficiency of the Kuhn-Tucker conditions for constrained minimization (7) of the linear form (6) with respect to $\tilde{\gamma}^\alpha$, which can be verified by a direct elementary proof. ∎

The above equivalence statement[46] in Lemma 1, based on the virtual work-rate expression (6), is fully general, that is, independent of any additional assumption.

In terms of the excess power $\tilde{w}^{\text{dist}} = \tilde{w} - \dot{w}$ locally supplied by a disturbing agency, inequality (7) on account of Equation $(3)_3$ simplifies to

$$\tilde{w}^{\text{dist}} = \tilde{w} - \dot{w} = -\sum_{\alpha\in\mathcal{N}} f^\alpha \tilde{\gamma}^\alpha \geq 0 \qquad \forall \tilde{\gamma}^\alpha \geq 0 \qquad \text{for given } \ \tilde{\mathbf{F}} = \dot{\mathbf{F}}. \tag{8}$$

The disturbance power $\tilde{w}^{\text{dist}}$ is zero if and only if $(\tilde{\gamma}^\alpha) \in \mathcal{L}$, where

$$\mathcal{L} := \{(\dot{\gamma}^\alpha) \mid \dot{\gamma}^\alpha \geq 0 \ \wedge \ \dot{\gamma}^\alpha = 0 \ \text{ if } f^\alpha \neq 0\}, \tag{9}$$

so that merely *potentially active* slip-systems are activated. That is,

$$\tilde{w} = \dot{w} = \mathbf{S}\cdot\dot{\mathbf{F}} \qquad \Leftrightarrow \qquad (\dot{\gamma}^\alpha) \in \mathcal{L}. \tag{10}$$

It follows that the minimum principle (7) determines the set (cone) $\mathcal{L}$ and is never sufficient to determine a unique nonzero solution $(\dot{\gamma}^\alpha)$ to Constitutive Rate-Problem (5) if applied in the current state $\mathcal{G}$ at a single instant only.

The minimum principle (7) admits a variety of extensions and generalizations, see a recent discussion in Reference 1.

2.3 | Quasi-extremal principle for the first-order work

Suppose that inequality (7) holds true in a given state $\mathcal{G}$ at time $t = 0$. Following Reference 1, apply now inequality (7) after a small time increment $\tau > 0$ along a solution path $(\dot{\mathbf{F}}(t), \dot{\gamma}^\alpha(t))$, so that

$$\tilde{w}^{\text{dist}}_\tau = -\sum_{\alpha\in\mathcal{N}} f^\alpha_\tau \tilde{\gamma}^\alpha \geq 0 \qquad \forall \tilde{\gamma}^\alpha \geq 0, \tag{11}$$

where a lower index τ indicates a quantity evaluated at time τ. It is assumed that all quantities vary continuously and sufficiently smoothly in the time interval $[0, \tau)$. With accuracy to the first order in τ, from the constitutive rate-equation $(2)_2$ we have

$$f^\alpha_\tau = f^\alpha + \tau\dot{f}^\alpha + o(\tau) = f^\alpha + \tau\left(\dot{\mathbf{F}}\cdot\mathbf{\Lambda}^\alpha - \sum_{\beta\in\mathcal{N}} g^{\alpha\beta}\dot{\gamma}^\beta\right) + o(\tau), \tag{12}$$

where $o(\tau)/\tau \to 0$ in the limit as $\tau \to 0$. It yields

$$\tilde{w}^{\text{dist}}_\tau(\tilde{\gamma}^\alpha, \dot{\gamma}^\alpha) = -\sum_{\alpha\in\mathcal{N}} f^\alpha\tilde{\gamma}^\alpha - \tau\sum_{\alpha\in\mathcal{N}}\left(\dot{\mathbf{F}}\cdot\mathbf{\Lambda}^\alpha - \sum_{\beta\in\mathcal{N}} g^{\alpha\beta}\dot{\gamma}^\beta\right)\tilde{\gamma}^\alpha \tag{13}$$

with accuracy to $o(\tau)$. The key point is that the above expression depends not only on virtual slip-rates $\tilde{\gamma}^\alpha$ but also on an unknown rate-solution $\dot{\gamma}^\alpha$. The function $\tilde{w}^{\text{dist}}_\tau$ is defined up to the first-order with respect to a time distance τ from the given state at $t = 0$, the leading term being independent of τ.

As a corollary from Reference 1(theorem 1), the following proposition holds true.

Proposition 1. *(Energy formulation of Constitutive Rate-Problem) The following statements are equivalent:*

(i) $(\dot{\gamma}^\alpha)$ *satisfies the quasi-extremal energy principle of first order (QEP1):*

$$(\dot{\gamma}^\alpha) = \arg\min_{\tilde{\gamma}^\alpha\geq 0} \tilde{w}^{\text{dist}}_\tau(\tilde{\gamma}^\alpha, \dot{\gamma}^\alpha) \qquad \text{for all } \ \tau \geq 0 \ \text{ sufficiently small.} \tag{14}$$

(ii) $(\dot{\gamma}^\alpha)$ *is a solution to Constitutive Rate-Problem (5).*

The proof is given in Reference 1 for a more general case that encompasses the present one.

2.4 | Quasi-extremal principle for the second-order work

Consider a deformation path that starts at time $t = 0$ from a given state $\mathcal{G}$ in which $\mathbf{S}, f^\alpha$ and all the state-dependent coefficients in Equations (2) are known. A short straight segment of the path is characterized by virtual rates $(\tilde{\mathbf{F}}, \tilde{\gamma}^\alpha)$ taken constant in a time interval $[0, \tau)$. The virtual work density per unit reference volume on that segment is defined as a time integral over $[0, \tau)$ of the virtual work-rate $\tilde{w}$. By the Taylor expansion of the integral up to the second-order terms with respect to τ, we obtain the following expression for the virtual work density:

$$w_\tau = w_1\tau + w_2\tau^2 + o(\tau^2), \qquad w_1 = \mathbf{S}\cdot\tilde{\mathbf{F}} - \sum_{\alpha\in\mathcal{N}} f^\alpha\tilde{\gamma}^\alpha, \qquad w_2 = \frac{1}{2}\tilde{\mathbf{S}}\cdot\tilde{\mathbf{F}} - \frac{1}{2}\sum_{\alpha\in\mathcal{N}}\tilde{f}^\alpha\tilde{\gamma}^\alpha. \tag{15}$$

By using Equation (2) with the normality flow rule reduced to $\mathbf{\Lambda}^\alpha_{\mathrm{p}} = \mathbf{\Lambda}^\alpha$, we have

$$\tilde{\mathbf{S}} = \mathbb{C}^{\mathrm{e}}\cdot\tilde{\mathbf{F}} - \sum_{\alpha\in\mathcal{N}}\mathbf{\Lambda}^\alpha\tilde{\gamma}^\alpha, \qquad \tilde{f}^\alpha = \tilde{\mathbf{F}}\cdot\mathbf{\Lambda}^\alpha - \sum_{\beta\in\mathcal{N}} g^{\alpha\beta}\tilde{\gamma}^\beta, \tag{16}$$

and w_2 is a quadratic form

$$w_2(\tilde{\gamma}^\alpha, \tilde{\mathbf{F}}) = \frac{1}{2}\sum_{\alpha,\beta\in\mathcal{N}}\tilde{\gamma}^\alpha g^{\alpha\beta}\tilde{\gamma}^\beta - \sum_{\alpha\in\mathcal{N}}\tilde{\mathbf{F}}\cdot\mathbf{\Lambda}^\alpha\tilde{\gamma}^\alpha + \frac{1}{2}\tilde{\mathbf{F}}\cdot\mathbb{C}^{\mathrm{e}}\cdot\tilde{\mathbf{F}}. \tag{17}$$

Now, following the main idea introduced in Reference 1, consider a short deformation path that leads to the same final increments $(\tau\tilde{\mathbf{F}}, \tau\tilde{\gamma}^\alpha)$ as above but consists of *two* straight segments, the first aligned with $\dot{\gamma}^\alpha$. It has been shown[1] that the decomposition (15) is then replaced with

$$w_\tau = w_1\tau + \varepsilon_2\tau^2 + o(\tau^2), \qquad \varepsilon_2(\tilde{\gamma}^\alpha, \tilde{\mathbf{F}}; \dot{\gamma}^\alpha) = w_2(\tilde{\gamma}^\alpha, \tilde{\mathbf{F}}) + \sum_{\alpha,\beta\in\mathcal{N}}\tilde{\gamma}^\alpha g^{\alpha\beta}_{\mathrm{skew}}\dot{\gamma}^\beta, \tag{18}$$

where $(g^{\alpha\beta}_{\mathrm{skew}})$ is a skew-symmetric part of $(g^{\alpha\beta})$,

$$g^{\alpha\beta}_{\mathrm{skew}} = \frac{1}{2}(g^{\alpha\beta} - g^{\beta\alpha}). \tag{19}$$

A detailed derivation of a similar function but extended to finite increments and containing additional terms is given in Appendix. If $(\tilde{\gamma}^\alpha) \in \mathcal{L}$ then for given $\tilde{\mathbf{F}} = \dot{\mathbf{F}}$ the term w_1 takes by Equation (10) a fixed value, and minimization of w_τ for τ sufficiently small reduces to minimization of ε_2.

From theorem 2 in Reference 1, if all current $f^\alpha \le 0$, we obtain the following corollary.

Proposition 2. *A solution to the quasi-extremal principle (QEP2) for the second-order energy function (18), namely*

$$(\dot{\gamma}^\alpha) = \arg\min_{(\tilde{\gamma}^\alpha)\in\mathcal{L}}\varepsilon_2(\tilde{\gamma}^\alpha, \dot{\gamma}^\alpha) \qquad \text{for given } \tilde{\mathbf{F}} = \dot{\mathbf{F}}, \tag{20}$$

solves Constitutive Rate-Problem (5) and satisfies additionally the path-stability condition

$$\sum_{\alpha,\beta\in\mathcal{N}}(\tilde{\gamma}^\alpha - \dot{\gamma}^\alpha)g^{\alpha\beta}(\tilde{\gamma}^\beta - \dot{\gamma}^\beta) \ge 0 \qquad \text{subject to } (\tilde{\gamma}^\alpha) \in \mathcal{L} \text{ and } \sum_{\alpha\in\mathcal{N}}\dot{f}^\alpha\tilde{\gamma}^\alpha = 0. \tag{21}$$

The proof is given in Reference 1 for a more general case that encompasses the present one.

Remark 1. The left-hand expression in inequality (21) can be interpreted[1] as the second-order work, supplied by a disturbing agency to the material that is *deforming* plastically with slip-rates $\dot{\gamma}^\alpha$, and associated with the change of the slip-rates to $\tilde{\gamma}^\alpha$. QEP2 (20) through condition (21) introduces thus an energetic condition for path stability, for a given velocity gradient $\dot{\mathbf{F}}$. Condition (21) implies positive semidefiniteness of the slip-system interaction submatrix $(\hat{g}^{\alpha\beta})(\dot{\gamma}) = (g^{\alpha\beta})$ restricted to the rows and columns corresponding to active slip-systems for which $\dot{\gamma}^\alpha > 0$ and $\dot{\gamma}^\beta > 0$. Solutions that violate this condition are rejected as describing an unstable path.

2.5 | Further specification of constitutive equations

The constitutive framework given in Section 2.1, while sufficient to construct the conceptual algorithm, is supplemented here with the typical assumptions of the conventional theory of crystal plasticity used in applications. The formulation adopted below follows Reference 7, where the reader can find more details and references to the literature. Although it is not necessary, the common multiplicative split of a finite deformation gradient $\mathbf{F}$ is used,[63]

$$\mathbf{F} = \mathbf{F}^*\mathbf{F}^{\mathrm{p}}, \quad \mathbf{F}^* = \mathbf{R}^*\mathbf{U}^{\mathrm{e}}, \qquad \det\mathbf{F}^* > 0, \quad \det\mathbf{F}^{\mathrm{p}} = 1, \tag{22}$$

where $\mathbf{F}^{\mathrm{p}}$ is the plastic deformation gradient, $\mathbf{F}^*$ is a contraction of the lattice rotation $\mathbf{R}^*$ and the elastic stretch tensor $\mathbf{U}^{\mathrm{e}}$ taken relative to the stress-free lattice configuration, and $\boldsymbol{\xi}$ denotes local internal variables of any type. For given $\mathbf{F}$, tensor $\mathbf{U}^{\mathrm{e}}$ depends on $\mathbf{F}^{\mathrm{p}}$, therefore $\mathbf{F}^{\mathrm{p}}$ acts as an internal variable additional to $\boldsymbol{\xi}$.

The attention is restricted to the case when elastic properties of the lattice are unaffected by plastic flow. Accordingly, the common split of the isothermal free energy function into the elastic strain energy function $\phi^{\mathrm{e}}(\mathbf{U}^{\mathrm{e}})$ of class C^2 and the residual part $\phi^{\mathrm{p}}(\boldsymbol{\xi})$ is assumed, namely,

$$\phi(\mathbf{F}^*, \boldsymbol{\xi}) = \phi^{\mathrm{e}}(\mathbf{U}^{\mathrm{e}}) + \phi^{\mathrm{p}}(\boldsymbol{\xi}) \qquad \text{and} \qquad \mathbf{S}^* = \frac{\partial\phi^{\mathrm{e}}}{\partial\mathbf{F}^*} \qquad \text{at constant temperature.} \tag{23}$$

The elastic stiffness pseudomoduli tensor $\mathbb{C}^{\mathrm{e}} = \overset{\mathrm{T}}{\mathbb{C}^{\mathrm{e}}} = \partial^2\phi/\partial\mathbf{F}\partial\mathbf{F}\big|_{\mathbf{F}^{\mathrm{p}}}$ (at fixed $\mathbf{F}^{\mathrm{p}}$), which appears in Equations (2) or (16), along with its counterpart $\mathbb{C}^* := \partial^2\phi^{\mathrm{e}}/\partial\mathbf{F}^*\partial\mathbf{F}^*$, can be determined by using the standard chain rule of differentiation and applying Equations (22). The Piola stress $\mathbf{S}$ is related to $\mathbf{S}^*$ through $\mathbf{S} = \mathbf{S}^*\overline{\mathbf{F}}^{\mathrm{T}}$.

The evolution equation for $\mathbf{F}^{\mathrm{p}}$ in crystal plasticity reads

$$\dot{\mathbf{F}}^{\mathrm{p}}(\mathbf{F}^{\mathrm{p}})^{-1} = \sum_{\alpha}\mathbf{m}^{\alpha}\otimes\mathbf{n}^{\alpha}\dot{\gamma}^{\alpha}, \tag{24}$$

where $(\mathbf{m}^{\alpha}, \mathbf{n}^{\alpha})$ is a pair of orthogonal unit vectors that define slip direction and slip-plane normal, respectively, in the stress-free (intermediate) configuration of the crystallographic lattice, assumed unaffected by changes in $\boldsymbol{\xi}$. The assumption $\mathbf{m}^{\alpha}\cdot\mathbf{n}^{\alpha} = 0$ implies that the plastic deformation is isochoric, $\det\mathbf{F}^{\mathrm{p}} \equiv 1$, by Jacobi's formula for the rate of $\det\mathbf{F}^{\mathrm{p}}$. The rate of $\boldsymbol{\xi}$ is assumed to be linearly related to $\dot{\gamma}^{\alpha}$ with state-dependent coefficients.

After known transformations which are omitted here, the generalized Schmid stress τ^{α}, such that $\sum_{\alpha}\tau^{\alpha}\dot{\gamma}^{\alpha}$ is the plastic work-rate per unit reference volume, reads

$$\tau^{\alpha} = \boldsymbol{\Pi}\cdot\mathbf{N}^{\alpha}, \qquad \mathbf{N}^{\alpha} = \mathbf{m}^{\alpha}\otimes\mathbf{n}^{\alpha}, \tag{25}$$

where $\boldsymbol{\Pi} = \overset{\mathrm{T}}{\mathbf{F}^*}\mathbf{S}^*$ is the Mandel stress.[64] The yield function f^{α} for αth slip-system is defined by

$$f^{\alpha} = \tau^{\alpha} - \tau^{\alpha}_{\mathrm{cr}}, \tag{26}$$

where $\tau^{\alpha}_{\mathrm{cr}}$ are the critical resolved shear stresses obeying the conventional incremental hardening law

$$\dot{\tau}^{\alpha}_{\mathrm{cr}} = \sum_{\beta}h^{\alpha\beta}\,\dot{\gamma}^{\beta}, \qquad h^{\alpha\beta} = \overline{h}^{\alpha\beta}(\boldsymbol{\xi}), \tag{27}$$

for given functions $\overline{h}^{\alpha\beta}$. Remarkably, the split of $\tau^{\alpha}_{\mathrm{cr}}$ into energetic and dissipative parts need not be specified here, so that the residual part $\phi^{\mathrm{p}}(\boldsymbol{\xi})$ of the free energy density remains arbitrary[7(remark 2)] as it does not affect the final constitutive equations nor the algorithm below.

The above constitutive equations are nowadays standard in conventional crystal plasticity at finite deformation. The adopted expressions for state-dependent coefficients in the evolution Equation $(16)_2$ for yield function f^{α} are less standard,[7] namely

$$\mathbf{\Lambda}^{\alpha} = \left(\mathbb{C}^{*} \cdot \mathbf{F}^{*}\mathbf{N}^{\alpha} + \mathbf{S}^{*}\overset{\mathrm{T}}{\mathbf{N}}{}^{\alpha} \right) \mathbf{F}^{\mathrm{P}-T}, \tag{28}$$

$$g^{\alpha\beta} = h^{\alpha\beta} + \mathbf{F}^{*}\mathbf{N}^{\alpha} \cdot \mathbb{C}^{*} \cdot \mathbf{F}^{*}\mathbf{N}^{\beta} + \mathbf{\Pi} \cdot \mathbf{N}^{\beta}\mathbf{N}^{\alpha}. \tag{29}$$

The last formula makes it explicit that matrix $(g^{\alpha\beta})$ is generally nonsymmetric for two independent reasons: $(h^{\alpha\beta}) \neq (h^{\beta\alpha})$ or $\mathbf{\Pi} \cdot (\mathbf{N}^{\beta}\mathbf{N}^{\alpha} - \mathbf{N}^{\alpha}\mathbf{N}^{\beta}) \neq 0$. By time differentiation of Equations (25) and $(23)_2$, it can be shown[65] that the constitutive rate Equation (2) with coefficients (28) and (29) are equivalent to those given originally in another form by Hill and Rice.[2]

3 | QEP FORMULATION FOR FINITE INCREMENTS

3.1 | A general framework

By replacing the rates with small but finite increments over a time step $[t_k, t_{k+1}]$, a *quasi-extremal principle* (QEP) for a discretized plasticity problem[1] takes the form

$$x = \arg\min_{z \in \mathbb{Z}} \mathcal{E}(z, x), \qquad z = (\tilde{q}, \tilde{\mu}), \qquad \mathbb{Z} = \mathbb{R}^{m} \times \mathbb{R}^{n}_{+}, \tag{30}$$

where the variable $z = (\tilde{q}, \tilde{\mu})$ contains virtual increments $\tilde{q} = q_{k+1} - q_k \in \mathbb{R}^m$ of generalized displacements and non-negative incremental plastic multipliers $\tilde{\mu} \in \mathbb{R}^n_+$. An index k denotes a quantity evaluated at t_k. A general characteristic feature of a quasi-extremal principle is that the minimized real-valued function $\mathcal{E}$ depends not only on variable z but also on an unknown solution x as a parameter. A particular energy-based form of function $\mathcal{E}$ has been derived in Reference 1. When evaluated with accuracy to second-order terms, function $\mathcal{E}$ is nonconvex in general. Its straightforward extension to small but finite increments takes a fully analogous form,

$$\mathcal{E}(z, x) = \tilde{E}(z) + z \cdot Cx, \qquad C = -C^{\mathrm{T}}, \tag{31}$$

where the leading term is the incremental energy function defined for isothermal irreversible processes by

$$\tilde{E} = \tilde{\Phi} + \tilde{\Omega} + \tilde{D}. \tag{32}$$

Here, a tilde over a symbol denotes a virtual increment (instead of a virtual rate), Φ is the Helmholtz free energy, Ω the potential energy of external loads, and $\tilde{D}$ is the incremental rate-independent dissipation in the case when all components of z vary proportionally with time during the time step $[t_k, t_{k+1}]$. The new term $z \cdot Cx$ in Equation (31) introduced in Reference 1 provides an extension of the incremental energy minimization method to the general class of nonpotential incremental problems. It is expressed through the antisymmetric part $C = \frac{1}{2}(A - A^{\mathrm{T}})$ of a governing matrix A in constitutive equations $(\tilde{Q}, \tilde{f}) = Ax + o(t_{k+1} - t_k)$ that relate an incremental solution x to increments $\tilde{Q}$ of generalized forces and $\tilde{f}$ of yield functions.

In the next section, QEP (30) is specialized for the rate-independent crystal plasticity. It will be shown that a solution x to QEP (30) formulated at a material point solves the local incremental quasi-static problem so that $\tilde{f}$ satisfies the discrete consistency conditions at the end of a time step.

Additionally, QEP (30) in its present incremental version imposes the energy condition of stability on a solution path in the sense that small perturbing forces perform a non-negative work on the deviation δx they induce in the solution.[1] QEP (30) with nonconvex $\mathcal{E}$ provides thus a criterion of choice among multiple solutions that is not based on arbitrarily assumed imperfections or random selection but can be given a physical meaning. For potential problems we have $C = 0$, and then QEP (30) reduces to direct minimization of $\tilde{E}(z)$ referred to as the incremental energy minimization,[66] initiated in Reference 67.

3.2 | Incremental QEP in single crystal plasticity

To extend the quasi-extremal principles presented in Section 2 for crystal plasticity to finite increments, consider a finite time interval $[t_n, t_{n+1}]$. A quantity ψ dependent on t and evaluated at $t \in (t_n, t_{n+1})$ will be denoted by $\psi_t := \psi(t)$, its

end-point values by $\psi_n := \psi(t_n)$ and $\psi_{n+1} := \psi(t_{n+1})$, and its increment in the interval $[t_n, t_{n+1}]$ by a prefix Δ, so that $\Delta\psi := \psi_{n+1} - \psi_n$. A forward slip rate $\dot\gamma^\alpha(t)$ in a time-discrete solution is assumed to be *constant* for $t \in [t_n, t_{n+1})$. The basic problem is to update the quantities known at instant t_n to t_{n+1} in a manner consistent with the constitutive equations provided in Section 2.

We apply an implicit backward-Euler difference scheme. Accordingly, the two sets of conditions (3) and (4) that define the basic rule of plastic slip-system activity in the rate-independent framework are reduced to the so-called discrete consistency conditions,

$$\Delta\gamma^\alpha \geq 0 \qquad \text{and} \qquad f^\alpha_{n+1} \leq 0 \qquad \text{and} \qquad f^\alpha_{n+1}\,\Delta\gamma^\alpha = 0 \qquad \forall \alpha \in \mathcal{N}. \tag{33}$$

For consistency with the constitutive rate equation $(2)_2$ upon substituting

$$\dot{\mathbf{F}} := \frac{\Delta\mathbf{F}}{\Delta t}, \qquad \dot\gamma^\alpha := \frac{\Delta\gamma^\alpha}{\Delta t}, \tag{34}$$

it is required that

$$f^\alpha_{n+1} - f^\alpha_n = \Delta\mathbf{F}\cdot\mathbf{\Lambda}^\alpha_{n+1} - \sum_{\beta\in\mathcal{N}} g^{\alpha\beta}_{n+1}\Delta\gamma^\beta + o(\Delta t), \qquad \alpha \in \mathcal{N}. \tag{35}$$

It is assumed that the coefficients $\mathbf{\Lambda}^\alpha_t$ and $g^{\alpha\beta}_t$ vary continuously with respect to time t, which implies the indicated accuracy of Equation (35). It is also assumed that $f^\alpha_n \leq 0$ from the previous time step, since otherwise the inequality $(33)_2$ could not be satisfied for Δt small enough.

$\Delta\gamma^\alpha$ plays the role of an incremental plastic multiplier identified with an unknown increment of slip on the αth slip-system. In the constitutive algorithm, an increment $\Delta\mathbf{F}$ of the deformation gradient is treated as given, although extensions to mixed loading conditions are possible.[7] The time-discrete counterpart to Constitutive Rate-Problem (5) of rate-independent crystal plasticity posed in Section 2.1 takes the following incremental form.

Incremental Problem. *Given the state* $\mathcal{G}_n$, $f^\alpha_n \leq 0, \Delta\mathbf{F}$ *and relationship* (35), *find* $\Delta\gamma^\alpha$ *that satisfy the conditions* (33) *for all* $\alpha \in \mathcal{N}$ *simultaneously.* (36)

Remark 2. In the limit as $\Delta t \to 0$, a solution to Incremental Problem (36) provides an *exact* solution to the basic rate problem (5) at t_n. Indeed, upon substituting Equations (34) and performing the limiting passage at $\Delta t \to 0$, Equation (35) and conditions (33) reduce precisely to Equation $(2)_2$ and conditions (3), respectively. Moreover, if $f_n = 0$ then $f^\alpha_{n+1}/\Delta t \leq 0$ tends in the limit to $\dot f^\alpha \leq 0$, while $f^\alpha_{n+1}\Delta\gamma^\alpha/(\Delta t)^2 = 0$ gives in the limit $\dot f^\alpha\dot\gamma^\alpha$, so that conditions (4) are also met. Hence, all the conditions of the rate problem 1 are fulfilled. Without the key assumption (35), the limiting passage to rate problem 1 would fail.

The following expression will be used to calculate f^α_{n+1} at time t_{n+1} on a discretized solution path:

$$f^\alpha_{n+1} := \tau^\alpha_{n+1} - \tau^\alpha_{\mathrm{cr}\,n+1}, \tag{37}$$

where τ^α_{n+1} is defined by Equation (25) as the projection of the Mandel stress $\mathbf{\Pi}_{n+1}$ on the αth slip-system dyad, while $\tau^\alpha_{\mathrm{cr}\,n+1}$ is calculated incrementally by using the hardening law (27); see Section 3.3 for more detail. The theoretical results below are obtained without appealing to Equation (37).

As the specification of a global quasi-potential $\mathcal{E}$ (Section 3.1) for the local (i.e., pointwise) Incremental Problem (36), we take *the incremental energy* $\Delta\varepsilon$. Following,[1] it is obtained from the work density functional Δw evaluated for a sharply bent ("dog-leg") path of $(\gamma^\alpha)(t)$ which consists of two straight segments, such that the first (longer) is aligned with the searched solution $\Delta\gamma^\alpha$ and the second (shorter) represents a strong variation of the first at its end.

The resulting formula for $\Delta\varepsilon$ is derived in Appendix in a nonstandard way by applying a *backward* time integration over $[t_n, t_{n+1}]$ of the work-rate expression along an arbitrary continuous and piecewise-smooth path of $(\mathbf{F}, \gamma^\alpha)(t)$ leading to increments $(\Delta\mathbf{F}, \tilde\gamma^\alpha)$, under the sole assumption of constant coefficients. Then, on evaluating the time integral for a dog-leg path mentioned above, the final formula (A9) has been derived which is an extension of the asymptotic formula (18) from Section 2 to finite increments. Formula (A9) is adopted here with the coefficients evaluated at t_{n+1} for a yet

unknown or approximate solution $\Delta\gamma^\alpha$ as a parameter. Accordingly,

$$\begin{aligned}\Delta\varepsilon(\tilde{\gamma}^\alpha, \Delta\mathbf{F}; \Delta\gamma^\alpha) = \mathbf{S}_{n+1}\cdot\Delta\mathbf{F} - \frac{1}{2}\Delta\mathbf{F}\cdot\mathbb{C}^{\mathrm{e}}_{n+1}\cdot\Delta\mathbf{F} - \sum_{\alpha\in\mathcal{N}}\left(f^\alpha_{n+1} - \boldsymbol{\Lambda}^\alpha_{n+1}\cdot\Delta\mathbf{F}\right)\tilde{\gamma}^\alpha \\ - \frac{1}{2}\sum_{\alpha,\beta\in\mathcal{N}}\tilde{\gamma}^\alpha g^{\alpha\beta}_{n+1}\,\tilde{\gamma}^\beta + \frac{1}{2}\sum_{\alpha,\beta\in\mathcal{N}}\tilde{\gamma}^\alpha(g^{\alpha\beta}_{n+1} - g^{\beta\alpha}_{n+1})\Delta\gamma^\beta.\end{aligned} \tag{38}$$

Using the expression (A10) for $\overline{\Delta w}$ determined for a *single* straight segment, $\Delta\varepsilon$ can be written down in a more compact form as the following function

$$\Delta\varepsilon(\tilde{\gamma}^\alpha, \Delta\mathbf{F}; \Delta\gamma^\alpha) = \overline{\Delta w}(\tilde{\gamma}^\alpha, \Delta\mathbf{F}) + \frac{1}{2}\sum_{\alpha,\beta\in\mathcal{N}}\tilde{\gamma}^\alpha(g^{\alpha\beta}_{n+1} - g^{\beta\alpha}_{n+1})\Delta\gamma^\beta, \tag{39}$$

where $\overline{\Delta w}$ is the work expression for a straight path of $(\gamma^\alpha)(t)$,

$$\overline{\Delta w}(\tilde{\gamma}^\alpha, \Delta\mathbf{F}) = \mathbf{S}_{n+1}\cdot\Delta\mathbf{F} - \sum_{\alpha\in\mathcal{N}} f^\alpha_{n+1}\Delta\gamma^\alpha - \Delta_2 w, \tag{40}$$

and $\Delta_2 w$ is the second-order work expression extended to finite increments,

$$\Delta_2 w(\tilde{\gamma}^\alpha, \Delta\mathbf{F}) = \frac{1}{2}\Delta\mathbf{F}\cdot\mathbb{C}^{\mathrm{e}}_{n+1}\cdot\Delta\mathbf{F} - \sum_{\alpha\in\mathcal{N}}\left(\boldsymbol{\Lambda}^\alpha_{n+1}\cdot\Delta\mathbf{F}\right)\tilde{\gamma}^\alpha + \frac{1}{2}\sum_{\alpha,\beta\in\mathcal{N}}\tilde{\gamma}^\alpha g^{\alpha\beta}_{n+1}\,\tilde{\gamma}^\beta. \tag{41}$$

It is pointed out that only the symmetric part of matrix $(g^{\alpha\beta}_{n+1})$ affects $\overline{\Delta w}$, and a skew part of $(g^{\alpha\beta}_{n+1})$ and parameter $\Delta\gamma^\alpha$ only affect the last term in Equation (38) or (39). Obviously,

$$\Delta\varepsilon(\Delta\gamma^\alpha, \Delta\mathbf{F}; \Delta\gamma^\alpha) = \overline{\Delta w}(\Delta\gamma^\alpha, \Delta\mathbf{F}). \tag{42}$$

Consider a variation of $\Delta\varepsilon$ with respect to arguments $(\tilde{\gamma}^\alpha, \Delta\mathbf{F})$ while the coefficients and parameter $\Delta\gamma^\alpha$ are kept fixed. From the constitutive rate equations (2) with $\boldsymbol{\Lambda}^\alpha_{\mathrm{p}} \equiv \boldsymbol{\Lambda}^\alpha$ it follows that infinitesimal variations $\delta\mathbf{S}_{n+1}$ and δf^α_{n+1} caused by variations $\delta\mathbf{F} \equiv \delta\mathbf{F}_{n+1}$ and $\delta\gamma^\alpha \equiv \delta\tilde{\gamma}^\alpha$ read

$$\delta\mathbf{S}_{n+1} = \mathbb{C}^{\mathrm{e}}_{n+1}\cdot\delta\mathbf{F} - \sum_{\alpha\in\mathcal{N}}\boldsymbol{\Lambda}^\alpha_{n+1}\delta\gamma^\alpha, \qquad \delta f^\alpha_{n+1} = \delta\mathbf{F}\cdot\boldsymbol{\Lambda}^\alpha_{n+1} - \sum_{\beta\in\mathcal{N}} g^{\alpha\beta}_{n+1}\delta\gamma^\beta \qquad \alpha\in\mathcal{N}. \tag{43}$$

After straightforward transformations, it follows that

$$\begin{aligned}\delta(\Delta\varepsilon) &= \mathbf{S}_{n+1}\cdot\delta\mathbf{F} - \sum_{\alpha\in\mathcal{N}} f^\alpha_{n+1}\delta\gamma^\alpha + \delta\mathbf{S}_{n+1}\cdot\Delta\mathbf{F} - \sum_{\alpha\in\mathcal{N}}\delta f^\alpha_{n+1}\tilde{\gamma}^\alpha \\ &\quad - \left(\mathbb{C}^{\mathrm{e}}_{n+1}\cdot\delta\mathbf{F} - \sum_{\alpha\in\mathcal{N}}\boldsymbol{\Lambda}^\alpha_{n+1}\delta\gamma^\alpha\right)\cdot\Delta\mathbf{F} + \sum_{\alpha\in\mathcal{N}}\left(\delta\mathbf{F}\cdot\boldsymbol{\Lambda}^\alpha_{n+1} - \frac{1}{2}\sum_{\beta\in\mathcal{N}}(g^{\alpha\beta}_{n+1} + g^{\beta\alpha}_{n+1})\,\delta\gamma^\beta\right)\tilde{\gamma}^\alpha \\ &\quad + \frac{1}{2}\sum_{\alpha,\beta\in\mathcal{N}}\delta\gamma^\alpha(g^{\alpha\beta}_{n+1} - g^{\beta\alpha}_{n+1})\Delta\gamma^\beta \\ &= \mathbf{S}_{n+1}\cdot\delta\mathbf{F} - \sum_{\alpha\in\mathcal{N}} f^\alpha_{n+1}\delta\gamma^\alpha - \frac{1}{2}\sum_{\alpha,\beta\in\mathcal{N}}\delta\gamma^\alpha(g^{\alpha\beta}_{n+1} - g^{\beta\alpha}_{n+1})(\tilde{\gamma}^\beta - \Delta\gamma^\beta)\end{aligned} \tag{44}$$

since the remaining terms cancel each other of account of Equations (43) and $\mathbb{C}^{\mathrm{e}}_{n+1} = \overset{\mathrm{T}}{\mathbb{C}}{}^{\mathrm{e}}_{n+1}$. Note that the last term vanishes if $\delta\gamma^\alpha \propto \tilde{\gamma}^\alpha - \Delta\gamma^\alpha$.

We arrive at a remarkable conclusion that

$$\mathbf{S}_{n+1} = \frac{\partial\Delta\varepsilon}{\partial\Delta\mathbf{F}}, \qquad f^\alpha_{n+1} = -\left.\frac{\partial\Delta\varepsilon}{\partial\tilde{\gamma}^\alpha}\right|_{\tilde{\gamma}^\beta = \Delta\gamma^\beta}, \tag{45}$$

so that function $\Delta\varepsilon$ acts precisely as a potential for $\mathbf{S}_{n+1}$ and a *quasi-potential* for f^{α}_{n+1}. This new result is a counterpart of a general equation[1 Eq. (72)] specialized here for finite slip increments in crystal plasticity.

Equation (44) provides the first-order Taylor decomposition of $\Delta\varepsilon$ with respect to variations of both $\Delta\mathbf{F}$ and $\tilde{\gamma}^{\alpha}$. Since incremental deformation gradient $\Delta\mathbf{F}$ is prescribed in the incremental problem (36), henceforth, we remove $\Delta\mathbf{F}$ from the list of variables to simplify the notation. The second variation of $\Delta\varepsilon$ in direction $\delta\gamma^{\alpha}$ for $\delta\mathbf{F}=\mathbf{0}$ reads

$$\delta^2(\Delta\varepsilon) = -\sum_{\alpha\in\mathcal{N}} \delta f^{\alpha}_{n+1}\delta\gamma^{\alpha} = \sum_{\alpha,\beta\in\mathcal{N}} \delta\gamma^{\alpha} g^{\alpha\beta}_{n+1}\delta\gamma^{\beta}. \tag{46}$$

The second-order Taylor series decomposition of $\Delta\varepsilon$ with respect to $\delta\gamma^{\alpha} := (\tilde{\gamma}^{\alpha} - \Delta\gamma^{\alpha})$, keeping $\Delta\mathbf{F}$, $\Delta\gamma^{\alpha}$ and the coefficients constant, takes thus the form

$$\Delta\varepsilon(\tilde{\gamma}^{\alpha}, \Delta\gamma^{\alpha}) = \Delta\varepsilon(\Delta\gamma^{\alpha}, \Delta\gamma^{\alpha}) + \Delta_1\varepsilon(\tilde{\gamma}^{\alpha}, \Delta\gamma^{\alpha}) + \Delta_2\varepsilon(\tilde{\gamma}^{\alpha}, \Delta\gamma^{\alpha}) + o(\tilde{\gamma}^{\alpha} - \Delta\gamma^{\alpha})^2, \tag{47}$$

with

$$\begin{aligned}
\Delta\varepsilon(\Delta\gamma^{\alpha}, \Delta\gamma^{\alpha}) &= \overline{\Delta w}(\Delta\gamma^{\alpha}), \qquad \Delta\mathbf{F} \text{ given},\\
\Delta_1\varepsilon(\tilde{\gamma}^{\alpha}, \Delta\gamma^{\alpha}) &= -\sum_{\alpha\in\mathcal{N}} f^{\alpha}_{n+1}(\tilde{\gamma}^{\alpha} - \Delta\gamma^{\alpha}),\\
\Delta_2\varepsilon(\tilde{\gamma}^{\alpha}, \Delta\gamma^{\alpha}) &= \frac{1}{2}\sum_{\alpha,\beta\in\mathcal{N}} (\tilde{\gamma}^{\alpha} - \Delta\gamma^{\alpha}) g^{\alpha\beta}_{n+1}(\tilde{\gamma}^{\beta} - \Delta\gamma^{\beta}).
\end{aligned} \tag{48}$$

This decomposition is not exact on account of the approximation involved in Equations (43) when infinitesimal variations are replaced with finite increments. Validity of decomposition (47) with accuracy to the second-order term $o(\tilde{\gamma}^{\alpha} - \Delta\gamma^{\alpha})^2$ can be verified by back-substitution of expressions (48) and (35) into Equation (47) and using Equation (43) as the first-order approximation.

In analogy to Reference 1(theorem 2) and Proposition 2 above, but with the modification due to finite increments, the following proposition holds true.

Proposition 3. *A solution* $(\Delta\gamma^{\alpha})$ *to the quasi-extremal energy principle (QEP) for finite increments:*

$$(\Delta\gamma^{\alpha}) = \arg\min_{\tilde{\gamma}^{\alpha}\geq 0} \Delta\varepsilon(\tilde{\gamma}^{\alpha}; \Delta\gamma^{\alpha}) \qquad \text{for given } \Delta\mathbf{F} \tag{49}$$

(i) solves Incremental Problem (36), and
(ii) satisfies additionally the condition

$$\sum_{\alpha,\beta\in\mathcal{N}} (\tilde{\gamma}^{\alpha} - \Delta\gamma^{\alpha}) g^{\alpha\beta}_{n+1}(\tilde{\gamma}^{\beta} - \Delta\gamma^{\beta}) \geq 0 \qquad \forall\tilde{\gamma}^{\alpha}\geq 0 \quad \text{subject to} \quad f^{\alpha}_{n+1}\tilde{\gamma}^{\alpha} = 0. \tag{50}$$

Proof. Suppose that there exists a vector $(\Delta\gamma^{\alpha})$ that solves QEP (49). Then $\Delta\varepsilon(\tilde{\gamma}^{\alpha}, \Delta\gamma^{\alpha}) \geq \Delta\varepsilon(\Delta\gamma^{\alpha}, \Delta\gamma^{\alpha})$ and from the Taylor decomposition (47) we obtain

$$\Delta_1\varepsilon(\tilde{\gamma}^{\alpha}, \Delta\gamma^{\alpha}) + \Delta_2\varepsilon(\tilde{\gamma}^{\alpha}, \Delta\gamma^{\alpha}) + o(\tilde{\gamma}^{\alpha} - \Delta\gamma^{\alpha})^2 \geq 0 \qquad \forall\tilde{\gamma}^{\alpha}\geq 0. \tag{51}$$

It follows that $\Delta_1\varepsilon(\tilde{\gamma}^{\alpha}, \Delta\gamma^{\alpha}) \geq 0$ for $|\tilde{\gamma}^{\alpha} - \Delta\gamma^{\alpha}|$ sufficiently small, which is possible if and only if the respective Kuhn–Tucker conditions (33) hold true. The consequence (i) is thus proven.

Suppose now that $\Delta_1\varepsilon(\tilde{\gamma}^{\alpha}, \Delta\gamma^{\alpha}) = 0$, which is the case if and only if $f^{\alpha}_{n+1}\tilde{\gamma}^{\alpha} = 0$ for each α on account of definition $(48)_2$ and conditions (33) obtained from (i). Then from inequality (51) it follows that $\Delta_2\varepsilon(\tilde{\gamma}^{\alpha}, \Delta\gamma^{\alpha}) \geq 0$, which yields the condition (ii). Proposition 3 has been proven. ∎

Remark 3. The left-hand expression in inequality (50) can be interpreted as the second variation of the energy function $\Delta\varepsilon$ in direction $\delta\gamma^{\alpha} = (\tilde{\gamma}^{\alpha} - \Delta\gamma^{\alpha})$, compare Equation (46). QEP (49) through condition (50) introduces thus an energetic condition for path stability, for a given increment $\Delta\mathbf{F}$ of the deformation gradient; compare also Remark 1 above. It means that the perturbation $(\delta\gamma^{\alpha})$ makes a negative scalar product with the associated perturbation (δf^{α}) for given $\Delta\mathbf{F}$, which can be interpreted as a contractivity property.

Remark 4. QEP (49) provides a criterion for the selection of active slip-systems, in the following sense. On physical grounds, when latent hardening exceeds self-hardening of slip systems, positive semidefiniteness of $(g^{\alpha\beta})$ can only be expected for linearly independent slip-systems whose number does not exceed 5.[10] Therefore, QEP (49) offers through condition (50) a criterion for eliminating the solution paths with more than five slip systems active simultaneously at one material point, which are unstable in the energy sense mentioned above. The basic advantage with respect to a similar method developed in Reference 7 is that QEP does *not* require the previous selective symmetrization of the slip-system interaction matrix $(g^{\alpha\beta})$.

Proposition 3 provides the theoretical basis for the algorithm developed in Section 4.

3.3 | Incremental update

Once Incremental Problem (36) has been solved (with any accuracy) with respect to $\Delta\gamma$, the update of a given local state $\mathcal{G}_n$ to $\mathcal{G}_{n+1}$ at time t_{n+1} follows straightforwardly from the constitutive equations given in Section 2.5. This incremental update is summarized in the set of Equations (52). It begins with the update of plastic deformation gradient $\mathbf{F}^{\mathrm{p}}$ calculated by using the exponential map, which preserves the plastic incompressibility and enables accurate calculation of the elastic deformation gradient $\mathbf{F}^{*}$.[68,69] The further equations follow from the constitutive framework given above.

$$
\begin{aligned}
\mathbf{F}_{n+1} &= \mathbf{F}_n + \Delta\mathbf{F},\\
\mathbf{F}^{\mathrm{p}}_{n+1} &= \exp\left(\sum_{\alpha}\Delta\gamma^{\alpha}\mathbf{N}^{\alpha}\right)\mathbf{F}^{\mathrm{p}}_{n},\\
\mathbf{F}^{*}_{n+1} &= \mathbf{F}_{n+1}\overset{\text{-1}}{\mathbf{F}^{\mathrm{p}}}_{n+1},\\
\mathbf{S}^{*}_{n+1} &= \frac{\partial\phi^{\mathrm{e}}}{\partial\mathbf{F}^{*}}(\mathbf{F}^{*}_{n+1}),\\
\mathbf{S}_{n+1} &= \mathbf{S}^{*}_{n+1}\overset{\text{-T}}{\mathbf{F}^{\mathrm{p}}}_{n+1},\\
\mathbf{\Pi}_{n+1} &= \overset{\text{T}}{\mathbf{F}^{*}}_{n+1}\mathbf{S}_{n+1}\overset{\text{T}}{\mathbf{F}^{\mathrm{p}}}_{n+1},\\
\tau^{\alpha}_{n+1} &= \mathbf{\Pi}_{n+1}\cdot\mathbf{N}^{\alpha},\\
\boldsymbol{\xi}_{n+1} &= \boldsymbol{\xi}_n + \Delta\boldsymbol{\xi}(\Delta\gamma^{\alpha}),\\
h^{\alpha\beta}_{n+1} &= \overline{h}^{\alpha\beta}(\boldsymbol{\xi}_{n+1}),\\
\tau^{\alpha}_{\mathrm{cr}\,n+1} &= \tau^{\alpha}_{\mathrm{cr}\,n} + \sum_{\beta}h^{\alpha\beta}_{n+1}\,\Delta\gamma^{\beta},\\
f^{\alpha}_{n+1} &= \tau^{\alpha}_{n+1} - \tau^{\alpha}_{\mathrm{cr}\,n+1},\\
\mathbb{C}^{*}_{n+1} &= \frac{\partial^2\phi^{\mathrm{e}}}{\partial\mathbf{F}^{*}\partial\mathbf{F}^{*}}(\mathbf{F}^{*}_{n+1}),\\
\mathbf{\Lambda}^{\alpha}_{n+1} &= \left(\mathbb{C}^{*}_{n+1}\cdot\mathbf{F}^{*}_{n+1}\mathbf{N}^{\alpha} + \mathbf{S}^{*}_{n+1}\overset{\text{T}}{\mathbf{N}}^{\alpha}\right)\overset{\text{-T}}{\mathbf{F}^{\mathrm{p}}}_{n+1},\\
g^{\alpha\beta}_{n+1} &= h^{\alpha\beta}_{n+1} + \mathbf{F}^{*}_{n+1}\mathbf{N}^{\alpha}\cdot\mathbb{C}^{*}_{n+1}\cdot\mathbf{F}^{*}_{n+1}\mathbf{N}^{\beta} + \mathbf{\Pi}_{n+1}\cdot\mathbf{N}^{\beta}\mathbf{N}^{\alpha}.
\end{aligned}
\tag{52}
$$

4 | THE ALGORITHM

4.1 | Relation to the incremental work minimization algorithm

A closer inspection shows that the minimized energy function $\Delta\varepsilon$ differs from the incremental work minimized in the previous approach,[7] including the algorithm refinement 1 given in the reference, only by the extra last term in Equation (38). This was not obvious in advance. This simple additional term plays a fundamental role as it removes the previous need for selective symmetrization of the slip-system interaction matrix $(g^{\alpha\beta})$. Mathematically, it is related to introducing a new

concept of a *quasi-extremal* principle in place of an extremal one. Nevertheless, the influence of this extra term on the structure of the computational algorithm given in Reference 7 turns out to be minor, and actually it leads to a simplification since the selective symmetrization step is now dropped. To make the present article self-contained, at the cost of unavoidable repetitions, the full description of the modified algorithm is provided in the next subsections. It is given in a condensed form, and the reader is referred to Reference 7 for more detailed explanations. Moreover, the algorithm can be extended to partial kinematic control in the same way, which is therefore not repeated here.

The expression (A11) for the second-order work extended to finite increments is repeated here for convenience:

$$\begin{aligned}\Delta_2 w &= \frac{1}{2}\Delta\mathbf{F}\cdot\mathbb{C}^{\mathrm{e}}\cdot\Delta\mathbf{F} - \sum_{\alpha\in\mathcal{N}}\left(\boldsymbol{\Lambda}^{\alpha}\cdot\Delta\mathbf{F}\right)\Delta\gamma^{\alpha} + \frac{1}{2}\sum_{\alpha,\beta\in\mathcal{N}}\Delta\gamma^{\alpha}g^{\alpha\beta}\,\Delta\gamma^{\beta}\\ &= \frac{1}{2}\hat{\Delta}\mathbf{S}\cdot\Delta\mathbf{F} - \frac{1}{2}\sum_{\alpha\in\mathcal{N}}\hat{\Delta}f^{\alpha}\Delta\gamma^{\alpha},\end{aligned} \tag{53}$$

where

$$\hat{\Delta}\mathbf{S} := \mathbb{C}^{\mathrm{e}}\cdot\Delta\mathbf{F} - \sum_{\alpha\in\mathcal{N}}\boldsymbol{\Lambda}^{\alpha}\Delta\gamma^{\alpha}, \quad \hat{\Delta}f^{\alpha} := \Delta\mathbf{F}\cdot\boldsymbol{\Lambda}^{\alpha} - \sum_{\beta\in\mathcal{N}}g^{\alpha\beta}\Delta\gamma^{\beta}. \tag{54}$$

Interestingly, on adding and simultaneously subtracting the *doubled* expression for $\Delta_2 w$, the incremental work (A10), calculated on a linear path of γ_t^{α} varying proportionally with time, is transformed to

$$\overline{\Delta w} = (\mathbf{S}_{n+1} - \hat{\Delta}\mathbf{S})\cdot\Delta\mathbf{F} - \sum_{\alpha\in\mathcal{N}}(f_{n+1}^{\alpha} - \hat{\Delta}f^{\alpha})\Delta\gamma^{\alpha} + \Delta_2 w. \tag{55}$$

In the actual calculations of a nonlinear problem, the assumption of constant coefficients $\mathbb{C}^{\mathrm{e}} = \overset{\mathrm{T}}{\mathbb{C}}{}^{\mathrm{e}}$, $\boldsymbol{\Lambda}^{\alpha}$ and $g^{\alpha\beta}$ no longer holds so that expressions (54) become only approximate for the actual finite increments $\Delta\mathbf{S} = \mathbf{S}_{n+1} - \mathbf{S}_n$, $\Delta f^{\alpha} = f_{n+1}^{\alpha} - f_n^{\alpha}$. By direct comparison, expression (55) turns out to be fully analogous to the algorithmic refinement of the work function adopted in Reference 7(Eq. (55)) to improve accuracy of the iterative solution. The previously postulated refinement is thus derived here in a natural way as the consequence of applying the *backward* integration scheme (A1).

On substituting the above equalities into Equation (A9), we obtain the following approximation for quasi-potential $\Delta\varepsilon$:

$$\hat{\Delta}\varepsilon(\tilde{\gamma}^{\alpha}, \hat{\Delta}\gamma^{\alpha}) := \hat{\Delta}w(\tilde{\gamma}^{\alpha}, \hat{\Delta}\gamma^{\alpha}) + \sum_{\alpha,\beta\in\mathcal{N}}\tilde{\gamma}^{\alpha}g_{\mathrm{skew}}^{\alpha\beta}\hat{\Delta}\gamma^{\beta}, \tag{56}$$

where

$$\begin{aligned}\hat{\Delta}w(\tilde{\gamma}^{\alpha}, \hat{\Delta}\gamma^{\alpha}) = (\mathbf{S}_{n+1} - \hat{\Delta}\mathbf{S})\cdot\Delta\mathbf{F} - \sum_{\alpha\in\mathcal{N}}(f_{n+1}^{\alpha} - \hat{\Delta}f^{\alpha})\tilde{\gamma}^{\alpha}\\ + \frac{1}{2}\Delta\mathbf{F}\cdot\mathbb{C}^{\mathrm{e}}\cdot\Delta\mathbf{F} - \sum_{\alpha\in\mathcal{N}}\left(\boldsymbol{\Lambda}^{\alpha}\cdot\Delta\mathbf{F}\right)\tilde{\gamma}^{\alpha} + \frac{1}{2}\sum_{\alpha,\beta\in\mathcal{N}}\tilde{\gamma}^{\alpha}g^{\alpha\beta}\,\tilde{\gamma}^{\beta}.\end{aligned} \tag{57}$$

Except $(\tilde{\gamma}^{\alpha})$, all other quantities are taken from the preceding subiteration for $(\Delta\gamma^{\alpha}) := (\hat{\Delta}\gamma^{\alpha})$ within time step $[t_n, t_{n+1}]$ and evaluated at t_{n+1} as in the energy expression (42). Its approximation (56) is used in Box 4 of the algorithm. It is the last term in Equation (56) which is new in comparison with the incremental work minimization algorithm.[7]

4.2 | Solving QEP by the augmented Lagrangian method

The minimization subproblem in QEP (49) has the form of nonsmooth and constrained nonconvex optimization. To solve that problem by reducing it to a *smooth and unconstrained* optimization problem, the *augmented Lagrangian method* is adopted. For the description of this method the reader is referred to References 70 and 71. In the present case, the problem (49) is reduced to a sequence of unconstrained minimization problems for the augmented Lagrangian of the form

$$L(\tilde{\gamma}^\alpha, \lambda^\alpha; \Delta\gamma^\alpha) := \Delta\varepsilon(\tilde{\gamma}^\alpha; \Delta\gamma^\alpha) + \sum_{\alpha\in\mathcal{N}} \psi_c^\alpha(\tilde{\gamma}^\alpha, \lambda^\alpha) \to \min_{\tilde{\gamma}^\alpha} \quad \text{for given } \Delta\mathbf{F}. \tag{58}$$

Additional variables here are Lagrange multipliers λ^α that enable the removal of the constraints $\tilde{\gamma}^\alpha \geq 0$ from (58). The *augmented* Lagrangian multipliers are defined by

$$\overline{\lambda}^\alpha := \lambda^\alpha + c\tilde{\gamma}^\alpha, \tag{59}$$

and the functions ψ_c^α by

$$\psi_c^\alpha(\tilde{\gamma}^\alpha, \lambda^\alpha) := \frac{1}{2c}\left(\left(\min(0, \overline{\lambda}^\alpha)\right)^2 - (\lambda^\alpha)^2\right) \tag{60}$$

$$= \begin{cases} \lambda^\alpha\tilde{\gamma}^\alpha + \frac{c}{2}(\tilde{\gamma}^\alpha)^2 & \text{if} \quad \overline{\lambda}^\alpha \leq 0, \\ -\frac{1}{2c}(\lambda^\alpha)^2 & \text{if} \quad \overline{\lambda}^\alpha > 0. \end{cases} \tag{61}$$

Here, $c > 0$ is a parameter which need *not* increase unboundedly to approach the exact solution to the original minimization subproblem included in QEP (49). Once a local minimum in the subproblem (58) has been calculated, the next iteration within the same time step is performed for updated values of $\Delta\gamma^\alpha$ and λ^α until the discrete consistency conditions (58) are satisfied with a desired accuracy. The Lagrange multipliers λ^α are updated following the standard rule of the augmented Lagrangian method[70,71]

$$\lambda^\alpha := \min\left(0, \lambda^\alpha + c\Delta\gamma^\alpha\right). \tag{62}$$

The reader is referred to Reference 7 for more details regarding the augmented Lagrangian approach to the crystal plasticity problem analogous to the present one. The augmented Lagrangian approach also proved useful in other algorithms for crystal plasticity, compare Reference 35.

4.3 | The structure of the algorithm

The overall structure of the algorithm given in Box 1 is analogous to that given in Reference 7. However, there is a substantial difference as the previous incremental work minimization has been replaced here by quasi-minimization of incremental energy $\Delta\varepsilon$. Related differences will appear in Boxes 2, 3, and 4 referred to in Box 1 and given in the next subsections.

BOX 1 The structure of the incremental constitutive algorithm for a time step $[t_n, t_{n+1}]$

- *Input*: new $\mathbf{F} = \mathbf{F}_{n+1}$, given $\mathbf{data}_n = \{\mathbf{F}_n, \mathcal{A}_n, \mathbf{F}_n^{\mathrm{p}}, \boldsymbol{\xi}_n, \tau_{\mathrm{cr}\ n}^\alpha, \boldsymbol{\Lambda}_n^\alpha, g_n^{\alpha\beta}\}$ at t_n.

1. Compute *elastic predictor*: $f_{\mathrm{tr}}^\alpha = f^\alpha$ and **par** for $\Delta\gamma^\alpha \equiv 0$ using Box 2;

   if $\exists\alpha\ f_{\mathrm{tr}}^\alpha > \varepsilon$ **then** go to 2 *(plastic step)*

   else set $\mathcal{A} := \emptyset$ and go to *Output (elastic step)*.

2. **if** $1 \leq |\mathcal{A}_n| \leq 5$ **then** compute $\Delta\gamma^\alpha$ using *equations solver* Box 3 for given $\mathcal{A}_n$

   else go to 3;

   if $\exists\alpha\ f^{\alpha\notin\mathcal{A}_n} > \varepsilon$ **or** $\Delta\gamma^{\alpha\in\mathcal{A}_n} = 0$ **then** go to 3

   else set $\mathcal{A} := \mathcal{A}_n$ and go to 4 *(old active systems set)* .

3. Compute $\Delta\gamma^\alpha$ by *quasi-minimization of incremental energy* $\Delta\varepsilon$ in Box 4 *(new active systems set $\mathcal{A}$)*.

4. Update **par** using Box 2.

- *Output*: $\mathbf{data}_{n+1} := \{\mathbf{F}, \mathcal{A}\} \cup \mathbf{par}$ for t_{n+1}, set $n := n + 1$ and **go to** *Input*.

4.4 | Incremental update for given increments of slips

The update procedure for given $\Delta\gamma^\alpha$ provided in Box 2 is simplified with respect to that in Reference 7 as the selective symmetrization is no longer needed. The procedure here is to much extent standard, only the update of the coefficients of the incremental constitutive equations in the form given here is not common. The update is applied in general in a subiteration loop within a given time increment; when the loop is completed then the final values of $\Delta\gamma^\alpha$ provide the update summarized in Section 3.3 for a time step $[t_n, t_{n+1}]$. The plastic deformation gradient $\mathbf{F}^{\mathrm{p}}$ is updated by using the exponential map to preserve plastic incompressibility and improve accuracy of calculations of the elastic deformation gradient $\mathbf{F}^*$.[68,69] The second Piola–Kirchhoff stress $\mathbf{T}^{\mathrm{e}}$ is determined as the partial derivative of elastic strain energy ϕ^{e} being a given function of the Green strain tensor $\mathbf{E}^{\mathrm{e}}$, with the local unstressed (intermediate) configuration taken as reference. The functions $\overline{\mathbb{C}}^*$ and $\overline{\mathbb{C}}^{\mathrm{e}}$ needed to determine current elastic pseudomoduli tensors $\mathbb{C}^*$ and $\mathbb{C}^{\mathrm{e}}$ (cf. Section 2.5) have a well-known form Reference 58. On calculating the Mandel stress $\mathbf{\Pi}$, the current value of each yield function $f^\alpha = \tau^\alpha - \tau^\alpha_{\mathrm{cr}}$ is determined by using the basic definitions $\tau^\alpha = \mathbf{\Pi}\cdot\mathbf{N}^\alpha$ and $\mathbf{N}^\alpha = \mathbf{m}^\alpha \otimes \mathbf{n}^\alpha$ along with the slip-system hardening law.

BOX 2 Update procedure for given $\Delta\gamma^\alpha$

• *Input:* new: $\mathcal{A}, \Delta\gamma^\alpha, \mathbf{F}$, given: $\mathbf{F}_n, \mathbf{F}^{\mathrm{p}}_n, \boldsymbol{\xi}_n, \tau^\alpha_{\mathrm{cr}\,n}$.

1. *Deformation*: $\mathbf{F}^{\mathrm{p}} := \exp\left(\sum_{\alpha\in\mathcal{A}} \Delta\gamma^\alpha\, \mathbf{N}^\alpha\right)\mathbf{F}^{\mathrm{p}}_n, \quad \mathbf{F}^* = \mathbf{F}\overset{-1}{\mathbf{F}^{\mathrm{p}}}, \quad \mathbf{E}^{\mathrm{e}} = \frac{1}{2}\left(\overset{\mathrm{T}}{\mathbf{F}^*}\mathbf{F}^* - \mathbf{1}\right)$

   Stresses: $\mathbf{T}^{\mathrm{e}} = \partial\phi^{\mathrm{e}}/\partial\mathbf{E}^{\mathrm{e}}, \quad \mathbf{S}^* = \mathbf{F}^*\mathbf{T}^{\mathrm{e}}, \quad \mathbf{\Pi} = \overset{\mathrm{T}}{\mathbf{F}^*}\mathbf{S}^*, \quad \tau^\alpha = \mathbf{\Pi}\cdot\mathbf{N}^\alpha$

   Elastic moduli: $\mathbb{L}^{\mathrm{e}} = \partial^2\phi^{\mathrm{e}}/\partial\mathbf{E}^{\mathrm{e}}\partial\mathbf{E}^{\mathrm{e}}, \quad \mathbb{C}^* = \overline{\mathbb{C}}^*(\mathbb{L}^{\mathrm{e}}, \mathbf{T}^{\mathrm{e}}, \mathbf{F}^*), \quad \mathbb{C}^{\mathrm{e}} = \overline{\mathbb{C}}^{\mathrm{e}}(\mathbb{C}^*, \mathbf{F}^{\mathrm{p}})$.

2. *Hardening moduli*:

   $\boldsymbol{\xi} := \boldsymbol{\xi}_n + \Delta\boldsymbol{\xi}(\Delta\gamma^\alpha), \quad h^{\alpha\beta} = \overline{h}^{\alpha\beta}(\boldsymbol{\xi})$

3. *Yield functions*:

   $\tau^\alpha_{\mathrm{cr}} := \tau^\alpha_{\mathrm{cr}\,n} + \sum_{\beta\in\mathcal{A}} h^{\alpha\beta}\,\Delta\gamma^\beta$

   $f^\alpha := \tau^\alpha - \tau^\alpha_{\mathrm{cr}}$.

4. *Incremental approximation of yield functions*:

   $\mathbf{\Lambda}^\alpha = (\mathbb{C}^*\cdot\mathbf{F}^*\mathbf{N}^\alpha + \overset{\mathrm{T}}{\mathbf{S}^*}\mathbf{N}^\alpha)\overset{-\mathrm{T}}{\mathbf{F}^{\mathrm{p}}}$

   $g^{\alpha\beta} = h^{\alpha\beta} + \mathbf{F}^*\mathbf{N}^\alpha\cdot\mathbb{C}^*\cdot\mathbf{F}^*\mathbf{N}^\beta + \mathbf{\Pi}\cdot\mathbf{N}^\beta\mathbf{N}^\alpha$

   $\hat{\Delta}f^\alpha = \mathbf{\Lambda}^\alpha(\mathbf{F} - \mathbf{F}_n) - \sum_{\beta\in\mathcal{A}} g^{\alpha\beta}\Delta\gamma^\beta$.

• *Output*: $\mathbf{par} := \{\mathbf{F}^{\mathrm{p}}, \boldsymbol{\xi}, \tau^\alpha_{\mathrm{cr}}, \mathbf{\Lambda}^\alpha, g^{\alpha\beta}\}, f^\alpha, \hat{\Delta}f^\alpha$.

4.5 | Incremental solution for a prescribed set of active slip-systems

It is emphasized that this step summarized in Box 3 only serves to speed up the calculations whenever possible, otherwise it is not necessary in the QEP algorithm.

The part of the algorithm provided in Box 3 represents essentially the known return mapping algorithm of multi-surface plasticity,[23] except that it is used in Box 1 exclusively in the case when the number of active slip-systems from the preceding time step takes a value from 1 to 5. Then the inverse of slip-system interaction submatrix $(g^{\alpha\beta}_{\mathcal{A}})$ is expected to exist, moreover, $(g^{\alpha\beta}_{\mathcal{A}})$ is expected to be positive definite, provided the active slip-systems are linearly independent,[10] so that the Newton-Raphson method can safely be used. It may happen that $\Delta\gamma^\alpha$ takes temporarily a negative value during iterations; then such a value is replaced with zero (keeping set $\mathcal{A} = \mathcal{A}_n$ fixed), that is, $\Delta\gamma^\alpha := \langle\Delta\gamma^\alpha\rangle$, where $\langle x\rangle = x$ for nonnegative x and zero otherwise. In case of no convergence to $\Delta\gamma^{\alpha\in\mathcal{A}_n} > 0$ within a prescribed number of iterations, for example, due to singularity of $(g^{\alpha\beta}_{\mathcal{A}})$, the quasi-minimization of incremental energy in Box 4 is invoked, see Box 1.

BOX 3 Solving the system of nonlinear equations for given $\mathcal{A}_n$

• *Input*: new: $\mathbf{F}$, given: $\mathbf{data}_n$ at t_n, $f^\alpha_{\rm tr}$ from elastic predictor.

1. *Initialization*: $g^{\alpha\beta} := g^{\alpha\beta}_n$, $\mathbf{\Lambda}^\alpha := \mathbf{\Lambda}^\alpha_n$, $f^\alpha := f^\alpha_{\rm tr}$, $\hat{\Delta}\gamma^{\alpha\in\mathcal{A}_n} := 0$, $\Delta\gamma^{\alpha\notin\mathcal{A}_n} := 0$.

2. Compute $\Delta\gamma^{\alpha\in\mathcal{A}_n}$ from the system of linear equations

$$\sum_{\beta\in\mathcal{A}_n} g^{\alpha\beta}(\Delta\gamma^\beta - \hat{\Delta}\gamma^\beta) = f^\alpha, \qquad \alpha\in\mathcal{A}_n.$$

3. Set $\hat{\Delta}\gamma^\alpha := \Delta\gamma^\alpha := \langle\Delta\gamma^\alpha\rangle$ for $\alpha\in\mathcal{A}_n$ and update f^α and $g^{\alpha\beta}$ using Box 2.

4. Accuracy check: **if** $\exists\alpha\ |f^{\alpha\in\mathcal{A}_n}| > \varepsilon$ **then** go to 2.

• *Output*: incremental slips $\Delta\gamma^\alpha$ for $\alpha\in\mathcal{A}_n$.

4.6 | Automatic selection of active slip-systems by QEP

Box 4 constitutes the core of the proposed algorithm for rate-independent crystal plasticity, based on the quasi-extremal energy principle QEP (49).

It overcomes the long-standing difficulty in rate-independent crystal plasticity in selecting the set of active slip systems, especially if the incremental problem has more than one solution which correspond to different sets of active slip-systems. In the previous paper,[7] the incremental energy minimization method[66] was applied, which required modification of the constitutive equations by symmetrization of the active slip-system interaction submatrix. In the present article based on the quasi-minimization of the incremental energy function, the need for symmetrization has been eliminated, which gives a significant benefit since the algorithm has become applicable to the original constitutive equations with a nonsymmetric slip-system interaction matrix. Nevertheless, the previous algorithm developed in Reference 7 turned out to be flexible in adaptation and merely needed a few changes related to the addition of the new last term in Equations (39) and (57) to the previous expression for the incremental work density.

BOX 4 Algorithm of quasi-minimization of incremental energy

• Input: $\Delta\mathbf{F} = \mathbf{F} - \mathbf{F}_n$, given $\mathbf{data}_n$ at t_n, $f^\alpha_{\rm tr}$ from *elastic predictor*,
if f^α is calculated using Box 3 **then** take f^α **else** $f^\alpha := f^\alpha_{\rm tr}$,
estimate potentially active slip-systems set $\mathcal{P} := \mathcal{A}_n \cup \{\alpha \mid f^\alpha \geq \varepsilon\}$.

1. *Initialization*:
$g^{\alpha\beta} := g^{\alpha\beta}_n$, $\mathbf{\Lambda}^\alpha := \mathbf{\Lambda}^\alpha_n$, $f^\alpha := f^\alpha_{\rm tr}$, $\hat{\Delta}\gamma^{\alpha\in\mathcal{P}} := 0$, $\Delta\gamma^{\alpha\notin\mathcal{P}} := 0$,
set parameter $c > 0$ and initial Lagrange multipliers $\lambda^{\alpha\in\mathcal{P}} := 0$.

2. *Energy quasi-minimization loop*:

2.1. Compute incremental slips $\Delta\gamma^{\alpha\in\mathcal{P}}$ by minimization of augmented Lagrangian:

$$\Delta\gamma^\alpha := \arg\min_{\tilde{\gamma}^\alpha}\left(\hat{\Delta}\varepsilon(\tilde{\gamma}^\alpha;\hat{\Delta}\gamma^\alpha) + \sum_\alpha \psi^\alpha_c(\tilde{\gamma}^\alpha,\lambda^\alpha)\right), \qquad \alpha\in\mathcal{P}$$

2.2. Update Lagrange multipliers $\lambda^\alpha := \min\{0, \lambda^\alpha + c\Delta\gamma^\alpha\}$ for $\alpha\in\mathcal{P}$

2.3. Set $\mathcal{A} := \{\alpha \mid \Delta\gamma^\alpha > 0\}$ and $\hat{\Delta}\gamma^\alpha := \Delta\gamma^\alpha$ for $\alpha\in\mathcal{P}$

2.4. **if** the first iteration after *Initialization* **then** $\mathcal{P} := \mathcal{A}$

2.5. Update f^α and $\mathbf{par} \supset \{g^{\alpha\beta}, \mathbf{\Lambda}^\alpha\}$ using Box 2

2.6. Accuracy check: **if** $\exists\alpha|f^{\alpha\in\mathcal{A}}| > \varepsilon$ **then** go to 2.

3. Final check: **if** $\exists\alpha f^{\alpha\notin\mathcal{A}} > \varepsilon$ **then** $\mathcal{P} := \mathcal{P}\cup\{\alpha \mid f^\alpha > \varepsilon\}$ and go to 1.

• *Output*: new $\mathbf{par}$ at t_{n+1} .

Here, the active slip-system set $\mathcal{A}$ is determined by performing quasi-minimization of the energy function over a set $\mathcal{P}$ of potentially active slip-systems that can be selected *a priori* only to reduce the computational effort. The set $\mathcal{A}$ is then obtained (point 2.3) as part of the solution to the minimization problem 2.1, in distinction to the approaches where $\mathcal{A}$ is *assumed* before solving the system of equations $f^{\alpha\in\mathcal{A}} = 0$.

In order to accelerate the computations, in Box 4 the set $\mathcal{P}$ is reduced as soon as possible (point 2.4) and subsequently enhanced only if needed (point 3). The augmented Lagrangian term ψ_c^α takes care of the nonnegativeness of $\Delta\gamma^\alpha$ in the final solution. In the energy quasi-minimization loop, the Lagrange multipliers are updated (point 2.2) simultaneously with the current approximate solution (point 2.3) and state parameter values (point 2.5). In the calculations performed, a constant parameter $c = 10^4$ GPa has been adopted.

Minimization of the smooth augmented Lagrangian (point 1.1) was implemented within the scientific computing environment *Mathematica* (http://www.wolfram.com). In the unconstrained search for a minimum of the Lagrangian, the embedded function *FindMinimum* that employs the usual Newton method has been used, taking advantage of the explicit knowledge of the gradient and Hessian of functions $\hat{\Delta}\epsilon$ and ψ_c^α from their definitions. In case when the Hessian is not positive definite, the line search or trust region methods are employed for appropriate step control during minimization.

5 | NUMERICAL EXAMPLES

5.1 | Simulation of simple shear

Effectiveness of the algorithm is demonstrated by numerical simulations of large deformation of a fcc single crystal under simple shear in different directions. The notation of 12 positive and 12 negative slip-systems ($N = 24$) is taken after Reference 72; a negative slip direction is denoted by an overbar, compare Table 1.

The slip-system hardening matrix $(h^{\alpha\beta})$ in Equation (27) is specified in the following form taken from Reference 73

$$h^{\alpha\beta} = \left(\chi^{\alpha\beta} + q\left(1 - \chi^{\alpha\beta}\right)\right) h^\beta, \tag{63}$$

where $\chi^{\alpha\beta} = 1$ for coplanar slip-systems and $\chi^{\alpha\beta} = 0$ otherwise, the latent-to-self hardening ratio $q = 1.4$, and the slip-hardening rate h^β as a function of the generalized Schmid stress τ^β on the βth slip system is expressed by the formula

$$h^\beta = h_0\left(1 - \frac{\tau_c^\beta}{\tau_s}\right)^a \qquad \text{for } \tau_c^\beta \le \tau_s. \tag{64}$$

Note that matrix $(h^{\alpha\beta})$ is not symmetric. The material parameters have been specified to fit the hardening curve for a high-purity Cu single crystal tested in the authors' home department.[74] The initial yield stress is set to $\tau_0 = 1$ MPa, initial hardening parameter $h_0 = 250$ MPa, saturation stress $\tau_s = 144$ MPa and exponent $a = 2$. The model is intended to describe Stages III and IV of strain hardening at room temperature while Stage I (easy glide) hardening is not accounted for. Elastic moduli of cubic symmetry, $C_{11} = 170$ GPa, $C_{12} = 124$ GPa, $C_{44} = 75$ GPa, used to determine a constant elastic moduli tensor $\mathbb{L}^e$ for Cu have been adopted after Reference 75.

The crystal response to uniform simple shear has been calculated for a fully prescribed deformation gradient $\mathbf{F}(\lambda) = \mathbf{1} + \lambda\,\mathbf{A}\otimes\mathbf{B}$, where symbol $\mathbf{1}$ means the second-order identity tensor, and loading parameter $\lambda(t)$ increased from 0 to 5 with constant increment $\Delta\lambda = \Delta t/\mathrm{s} = 10^{-2}$. It was checked that decreasing the step size to $\Delta\lambda = 10^{-3}$ or $\Delta\lambda = 10^{-4}$ has no significant influence on the results. The calculations were performed for four orientations of simple-shear deformation as in Reference 76. Unit vectors of direction $\mathbf{A}$ and plane $\mathbf{B}$ of simple shear are defined relative to a fixed laboratory frame $\overline{X}_i$, $i = 1, 2, 3$, as in Table 2.

TABLE 1 Notation of planes and directions of slip-systems in fcc single crystals, adopted after Reference 72

a	**1**	**2**	**3**	***b***	**1**	**2**	**3**	***c***	**1**	**2**	**3**	***d***	**1**	**2**	**3**
(111)	$[0\bar{1}1]$	$[10\bar{1}]$	$[\bar{1}10]$	$(\bar{1}\bar{1}1)$	[011]	$[\bar{1}0\bar{1}]$	$[1\bar{1}0]$	$(\bar{1}11)$	$[0\bar{1}1]$	$[\bar{1}0\bar{1}]$	[110]	$(1\bar{1}1)$	[011]	$[10\bar{1}]$	$[\bar{1}\bar{1}0]$

TABLE 2 Orientations of unit vectors **A** and **B**, denoting direction and plane of simple-shear deformation relative to a fixed laboratory frame $\overline{X}_i$, $i = 1, 2, 3$

	(1)	(2)	(3)	(4)
A	[100]	[100]	[100]	[110]
B	(001)	(013)	(011)	(001)

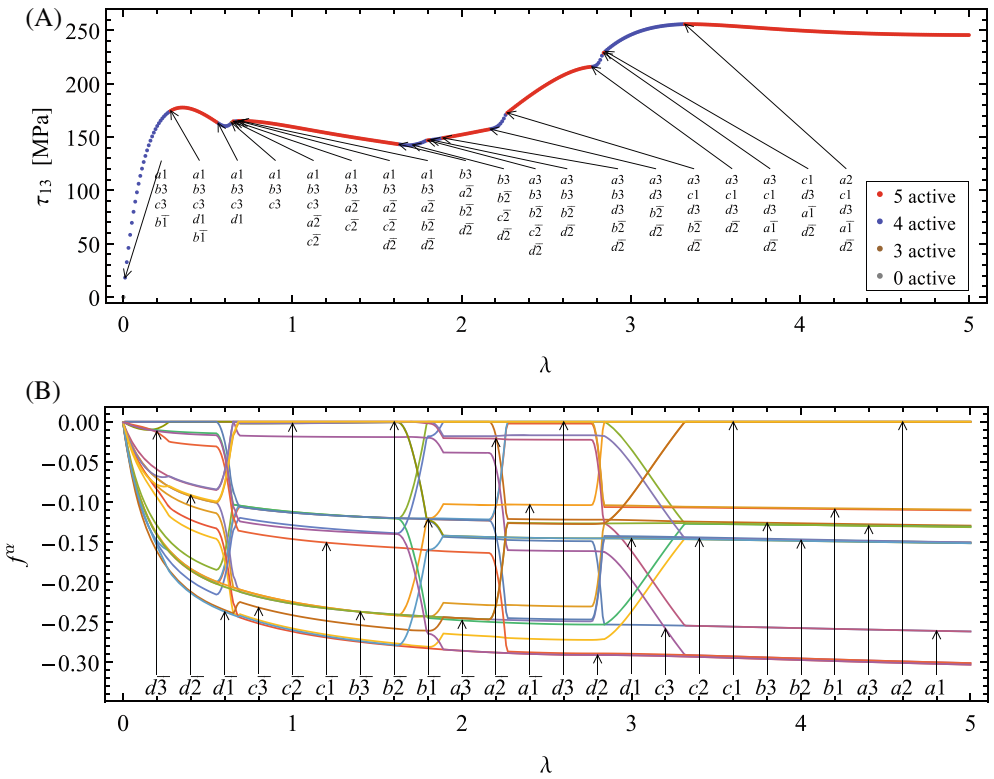

FIGURE 1 Simulation of simple shear No. (1): (A) shear stress τ_{13} versus shear strain with the active slip-system sets marked, and (B) corresponding values of the yield functions f^α for all slip-systems

The material response to the simple shear No. (1) is quite complex. In Figure 1A the plot of the Kirchhoff stress τ_{13} versus shear strain λ is shown along with the changing set of active slip-systems. Arrows indicate points where a new active slip-system set has been selected by the QEP algorithm. Different colors along the stress-strain curve mean different numbers of active slip-systems. Remarkably, the number of simultaneously active slip-systems never exceeds five. Four or five slip-systems are active throughout almost all the deformation stages. In a high-symmetry initial orientation, as in the case examined, several *equivalent* solutions exist, and the one presented here should be interpreted as a representative example.

For the chosen deformation step size $\Delta\lambda = 10^{-2}$, the initial elastic state is overshot, and immediately at the beginning of calculations the plastic state is reached. Changes of active sets occur frequently and as a rule are related to the appearance of some irregularities on the stress curves. The changes of active slip-systems are more visible on the plots of yield functions f^α, Figure 1B, when they reach or leave the zero level. The mechanism of automatic switching between different active slip-system sets is analogous to that described in detail in Reference 7, but this time without any symmetrization of the slip-system interaction matrix. The irregularities on the stress and yield functions f^α plots are related to the transition between corners of the yield surface. In particular, the irregularities are associated with unloading of slip-systems, which is clearly visible in Figure 1B.

Accumulated slips γ^α on individual slip-systems versus shear strain are plotted in Figure 2A. In the stage of deformation related to successive transitions between yield-surface corners the crystal lattice is subjected to large rotation, Figure 2B. Changes in the orientation of three crystallographic directions [100], [010], [001] are shown on the pole figure,

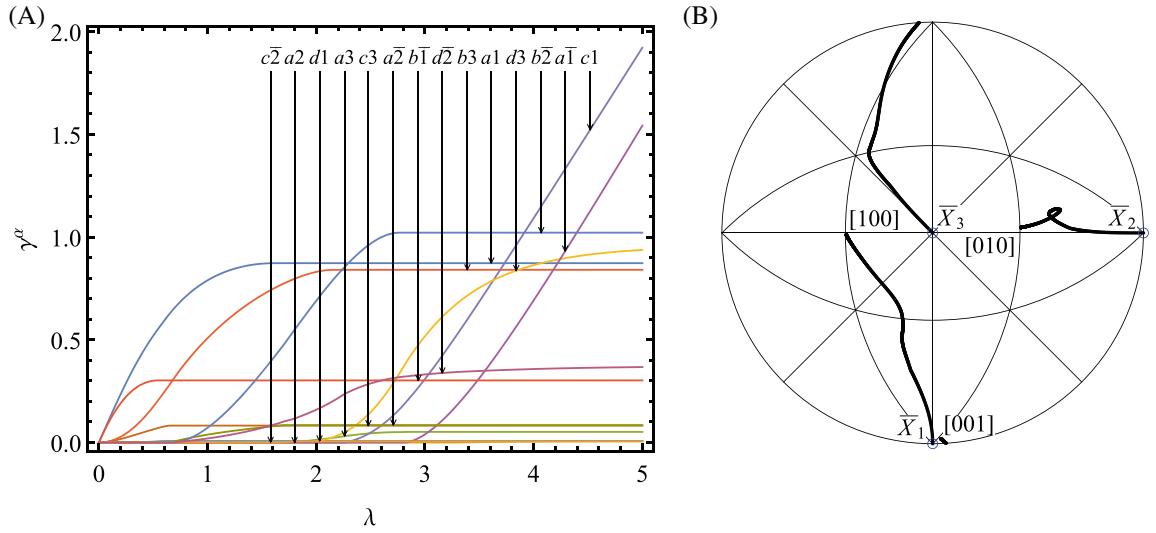

FIGURE 2 Simulation of simple shear No. (1): (A) accumulated slips on active slip-systems and (B) changes in the orientation of crystallographic axes

from their initial orientations $\overline{X}_1, \overline{X}_2, \overline{X}_3$ marked with circles. It can be seen from Figure 2A that slip-systems which are active at the beginning are later unloaded, as a result of rotation of the crystallographic lattice. In the final stage of the simulations, two slip-systems $(c1, a\bar{1})$ become dominant, and the remaining active systems are much slower. The rotation of the crystallographic lattice gradually slows down at the final stage of the simulation. It is worth recalling that during the entire deformation process no more than five simultaneously active slip-systems have been allowed by the path stability criterion embedded in the QEP algorithm.

In turn, the simple shear deformation No. (2) corresponds to a more localized, clearly visible irregularity on the shear stress τ_{13} and yield functions f^α plots in Figure 3. Only one change of a yield-surface corner appears in this deformation

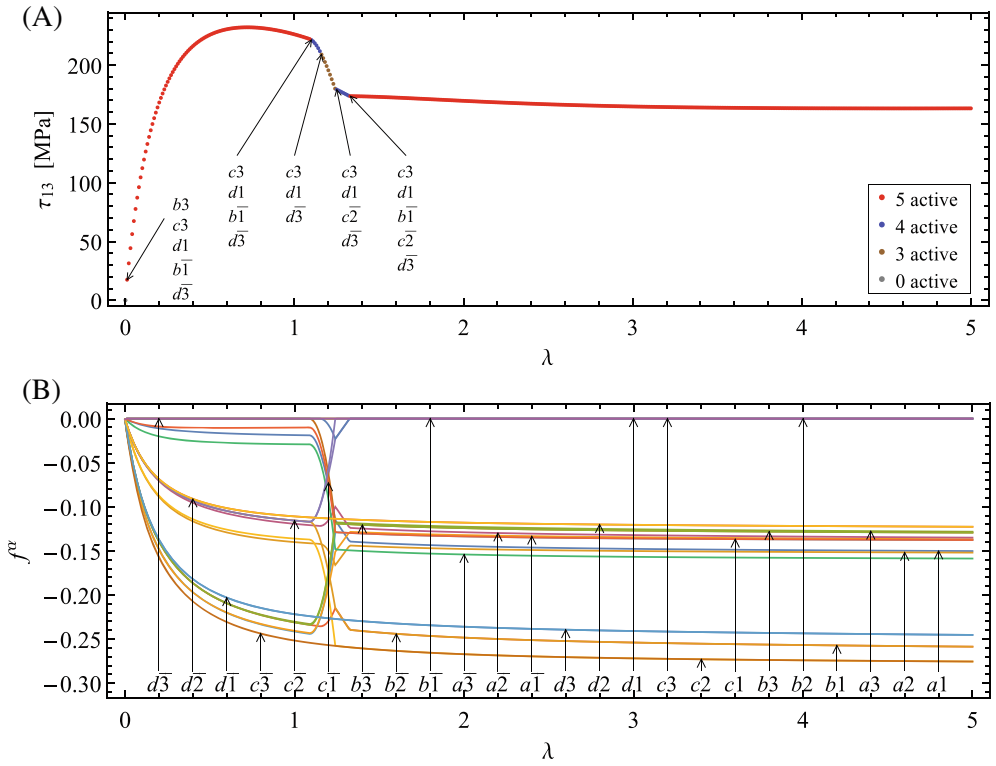

FIGURE 3 Simulation of simple shear No. (2): (A) shear stress τ_{13} versus shear strain with the active slip-system sets marked, and (B) corresponding values of the yield functions f^α for all slip-systems

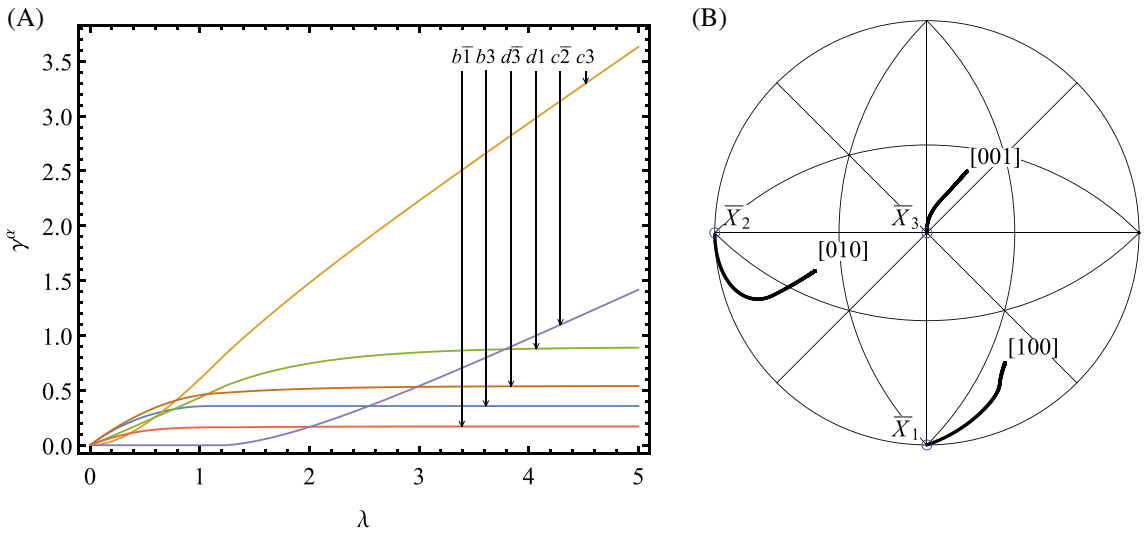

FIGURE 4 Simulation of simple shear No. (2): (A) accumulated slips on active slip-systems and (B) changes in the orientation of crystallographic axes

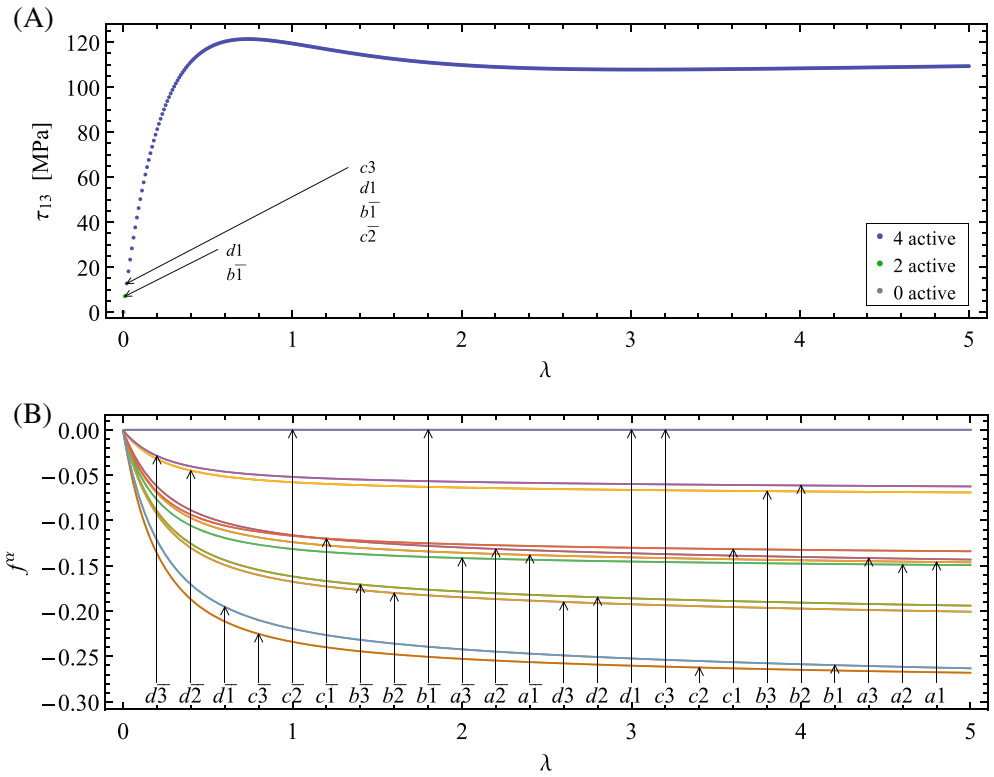

FIGURE 5 Simulation of simple shear No. (3): (A) shear stress τ_{13} versus shear strain with the active slip-system sets marked, and (B) corresponding values of the yield functions f^α for all slip-systems

process. It starts around $\lambda = 1.1$, when first $b3$ and next $b\bar{1}$ slip-systems become unloaded, and ends about $\lambda = 1.33$ when new slip-systems $c3$ and $c\bar{2}$ become active. Five slip-systems are active during the most part of the deformation, and after $\lambda = 1.33$ the set $(c3, d1, b\bar{1}, c\bar{2}, d\bar{3})$ is active. However, at the final stage two slip-systems $(c3, c\bar{2})$ are dominant, Figure 4A. The rotation of the crystallographic lattice Figure 4B runs more regularly compared to the previous deformation No. (1).

The simple shear deformation No. (3) visualized in Figure 5 is even more smooth and continues without any visible irregularities observed in the previous deformations No. (1) and No. (2). In the first step of deformation, two collinear systems $d1$ and $b\bar{1}$ starts to flow with equal increments of slip shearing. Shortly thereafter, in the second deformation

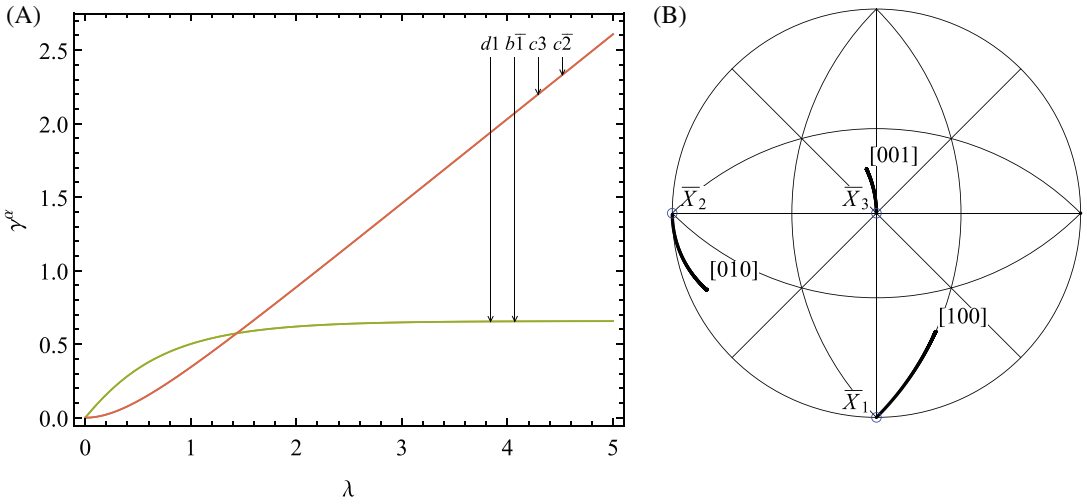

FIGURE 6 Simulation of simple shear No. (3): (A) accumulated slips on active slip-systems and (B) changes in the orientation of crystallographic axes

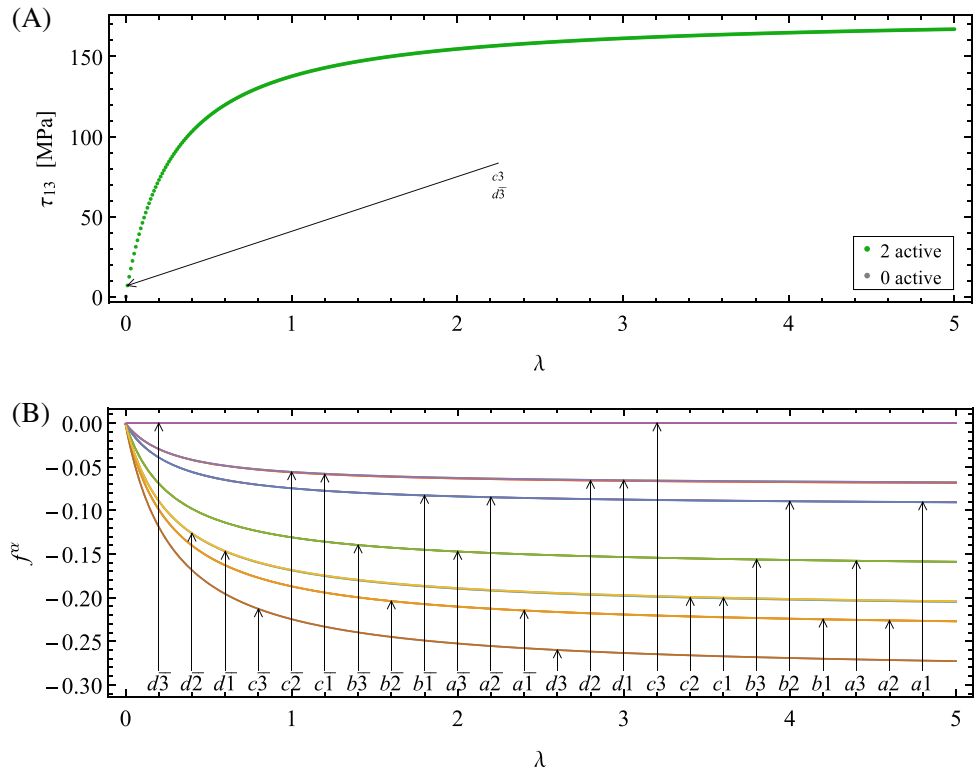

FIGURE 7 Simulation of simple shear No. (4): (A) shear stress τ_{13} versus shear strain with the active slip-system sets marked, and (B) corresponding values of the yield functions f^α for all slip-systems

step, two additional coplanar slip-systems $c3$ and $c\bar{2}$ are activated, which initially flow more slowly than the previous two slip-systems. As a result of the progressing smooth rotation of the lattice, Figure 6, the dominant role in the plastic flow is taken over by $c3$ and $c\bar{2}$ coplanar systems. The rotation of the lattice, accompanied by apparent geometric "softening", gradually decreases during deformation. No transition between yield-surface corners is observed and no slip-system is unloaded, so that the yield function values f^α vary smoothly and monotonically, Figure 5B.

Finally, the case of simple shear deformation No. (4) is extremely simple as the saturation type hardening on the shear stress τ_{13} curve occurs during the entire deformation, Figure 7A. Only two collinear slip-systems $c3$ and $d\bar{3}$, which undergo

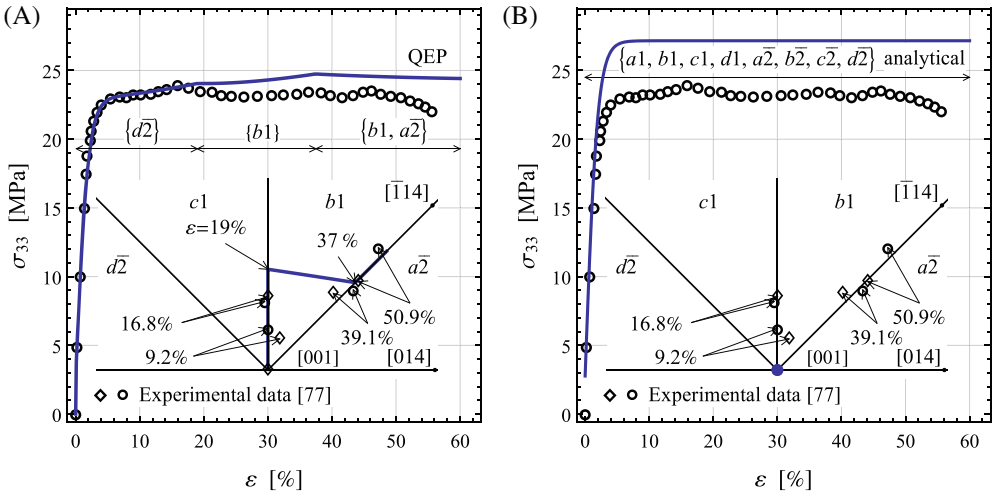

FIGURE 8 Tensile true stress versus engineering strain, active slip-systems and changes in the orientation of tensile axis for latent-hardening parameter $q = 1.2$, in comparison with experimental results from Reference 77. (A) Simulations for selecting active slip-systems by QEP, (B) analytical predictions with no criterion of slip-system selection

self and latent hardening, are active in the entire plastic range, while the remaining systems are inactive. The almost constant and equal increase of shearing of two slip-systems gives the same accumulated value of slips on both systems. The crystal lattice does not rotate, and accordingly there is no transition between yield-surface corners, Figure 7B. This particular case, unlike the previous three, can be treated by elementary analysis and is given here only to facilitate the interpretation of the previous figures generated by the same computer code.

5.2 | Uniaxial tension in high-symmetry orientation

From the point of view of the slip-system selection procedure, this example may be treated as a benchmark for crystal plasticity algorithms. For uniaxial tension of a fcc crystal in [001] direction, there are eight equally stressed slip-systems. If no criterion of slip-system selection is involved, simultaneous and equal activity of the eight slip-systems is predicted. This is in variance with experimental observations of a smaller number of simultaneously active slip-systems in a small volume element of a tensile specimen (the latter may deform nonuniformly). Such observations are well documented in the work[77] taken below as reference.

Numerical simulations of a uniaxial tension in a high-symmetry initial direction [001] have been previously performed using the incremental work minimization algorithm along with selective symmetrization of the slip-system hardening matrix.[7] This required the extension of the algorithm to the case of partial kinematic control. In those calculations, in order to obtain good agreement with the experimental results given in Reference 77, it was found necessary to assume two different latent-hardening parameters, $q_{\mathrm{lc}} = 1.3$ for slip-system pairs with sessile junctions and $q = 1.2$ for other pairs. It is shown below that the QEP algorithm, where the selective symmetrization is no longer used, allows the previous results to be accurately reproduced using only one latent-hardening parameter $q = 1.2$ and the other material parameters adopted from section 6.3 of Reference 7.

The material parameters have been assumed to fit the first portion of the experimental tension curve taken from References 77 for Al 99.99% single crystal of [100] initial orientation, shown as circle points in Figure 8. Saturation type hardening has been adopted in the form $h^{\beta}(\Gamma) := h_0 \operatorname{sech}^2\left(\frac{h_0\Gamma}{\tau_{\mathrm{s}}-\tau_0}\right)$ for every slip-system β after Reference 3, where accumulated shear Γ on all slip-systems is updated using the formula $\Gamma_{n+1} := \Gamma_n + \sum_{\alpha} \Delta\gamma^{\alpha}$. Formula (63) is applied here by taking $q = 1.2$ for latent hardening and $\chi^{\alpha\beta} = \delta^{\alpha\beta}$, the Kronecker delta. Simulations have been carried out for the initial yield stress $\tau_0 = 1.13$ MPa, saturation stress $\tau_{\mathrm{s}} = 8.5\tau_0$, initial hardening modulus $h_0 = 160\tau_0$, and elasticity moduli $C_{11} = 108$ GPa, $C_{12} = 62$ GPa, $C_{44} = 28$ GPa.

The uniaxial tension has been simulated by increasing loading parameter $\lambda(t)$ from 0 to 0.6 using step size $\Delta\lambda = 10^{-3}$. The QEP algorithm presented in Section 4 has been extended to the case of partial kinematic control in close analogy to the approach described in sections 6.1 and 6.2 of References 7. For uniaxial tension, the deformation gradient and Piola stress tensors are taken in the form

$$\mathbf{F} = \begin{bmatrix} \tilde{F}_{11} & 0 & 0 \\ \tilde{F}_{21} & \tilde{F}_{22} & 0 \\ \tilde{F}_{31} & \tilde{F}_{32} & \lambda \end{bmatrix}, \qquad \mathbf{S} = \begin{bmatrix} 0 & 0 & 0 \\ 0 & 0 & 0 \\ 0 & 0 & \tilde{S}_{33} \end{bmatrix}. \tag{65}$$

Components $\tilde{F}_{ij}$ and $\tilde{S}_{33}$ are unknown and determined at each step of λ along with the incremental shears $\Delta\gamma^\alpha$ by quasi-minimization of the energy function $\Delta\epsilon$ (for zero potential energy of external loads).

In the first stage of elongation up to the engineering strain $\varepsilon = \lambda - 1 = 19\%$, a single slip-system $d\bar{2}$ (as one of eight systems $\{a1, b1, c1, d1, a\bar{2}, b\bar{2}, c\bar{2}, d\bar{2}\}$ which are equivalent by symmetry) is activated. Stable rotation of the crystallographic lattice in (010) plane is observed, and the tensile direction rotates from initial direction [001] along $[001] - [\bar{1}01]$ vertical line until reaching the elongation $\varepsilon = 19\%$. Due to latent hardening, neither $b1$ nor $c1$ slip-systems are activated up to this point. Subsequently, the algorithm enforces the replacement of the active slip-system by $b1$ (an equivalent alternative would be $c1$) while $d\bar{2}$ is deactivated. The direction of lattice rotation changes, now the elongation direction is rotating toward $[001] - [\bar{1}11]$ line until reaching $\varepsilon = 37\%$ of elongation. Additional slip-system $a\bar{2}$ is then activated at the elongation $\varepsilon = 37\%$, and simultaneously one more abrupt change in the lattice rotation direction takes place. Two slip-systems $\{b1, a\bar{2}\}$ remain active while the tensile direction is now rotating along $[001] - [\bar{1}11]$ line.

The numerical simulations have been compared to the experimental results given by Saeki and Miura[77] for a tensile specimen of Al 99.99% single crystal of [100] initial orientation. The agreement between numerical and experimental stress-strain curves in Figure 8A is not perfect but may be regarded as satisfactory. Of more interest for validation of the slip-system selection is the comparison, inserted in Figure 8A, of the calculated crystal lattice rotations (shown as blue solid-line representing changes in the orientation of tensile axis on the inverse pole figure) with experimentally observed results. Two symmetry-related sets of experimental points for tensile axis rotations taken for two different regions of the specimen from Reference 77 are superimposed at one side of the vertical line and represented by diamonds and circles, labeled by the respective values of the sample elongation. In view of the observed complexity of the material response, and of simplicity of the material model, the obtained good agreement supports validity of the active slip-system selection based on the energetic criterion of path stability embedded in the QEP algorithm.

In contrast, if no criterion of slip-system selection is used then for uniaxial tension in [001] direction simultaneous and equal activity of the eight slip-systems $\{a1, b1, c1, d1, a\bar{2}, b\bar{2}, c\bar{2}, d\bar{2}\}$ indexed by $\alpha \in \mathcal{N}_{[001]}$ is predicted, which leads to the results presented in Figure 8B. In this case, there is no lattice rotation, and by disregarding a negligible effect of elastic strain, the crystal response can be determined analytically. Straightforward integration of formula (27) from the initial value $\tau^\alpha_{\rm cr} = \tau_0$, using hardening matrix (63) with h^β and $\chi^{\alpha\beta}$ specified earlier in this section, yields

$$\tau^\alpha_{\rm cr}(\Gamma) = \tau_0 + ((7/8)(q-1)+1)(\tau_{\rm s} - \tau_0)\tanh[\Gamma h_0/(\tau_{\rm s} - \tau_0)] \qquad \text{for } \alpha \in \mathcal{N}_{[001]}. \tag{66}$$

On substituting the expressions for resolved shear stress $\tau^\alpha = \sigma_{33}/\sqrt{6} = \tau^\alpha_{\rm cr}$ and accumulated plastic slip $\Gamma = \sqrt{6}\ln\lambda$, we arrive at the closed-form formula for σ_{33} versus λ,

$$\sigma_{33} = \sqrt{6}\left(\tau_0 + ((7/8)(q-1)+1)(\tau_{\rm s} - \tau_0)\tanh[\sqrt{6}\, h_0 \ln\lambda/(\tau_{\rm s} - \tau_0)]\right), \tag{67}$$

for the above rigid-plastic model of uniaxial tension in [001] direction with eight equally active slip-systems.

This analytical relationship is plotted in Figure 8B in terms of $\varepsilon = \lambda - 1$ for the material parameters given above. The curve is clearly higher than in Figure 8A due to the higher contribution of latent hardening. The most noteworthy, however, is the discrepancy between the predicted fixed orientation of the tensile axis, marked by a bold center point in the inverse pole figure, and its experimentally observed rotations marked with diamonds and circles. The discrepancy

occurs irrespective of the values of the material parameters if there is no built-in mechanism of slip-system selection that could enforce a deviation from the initially imposed symmetry.

5.3 | Comparison with other algorithms

We begin with the example of uniaxial tension in high-symmetry orientation [001] as in the preceding Section 5.2.

The same slip-systems as in Figure 8A were active in the calculations performed in Reference 7 for two different latent-hardening parameters ($q = 1.2$ and $q_{\mathrm{lc}} = 1.3$) assumed under otherwise the same material model. The slip-system selection in the reference was also based on the energy criterion of path stability, but understood together with the concept of selective symmetrization, not used here. Nevertheless, the results given in figure 7(a) in Reference 7 practically coincide with these in Figure 8A here.

When using a standard rate-dependent model (RD), the results are fundamentally different. The reason is that in the absence of imperfections other than round-off errors, during uniaxial tension in [001] direction there is no mechanism in the RD calculations for deviation from the equal activity of the eight equally stressed slip systems $\{a1, b1, c1, d1, a\overline{2}, b\overline{2}, c\overline{2}, d\overline{2}\}$. In effect, rotations of the crystallographic lattice are absent, and for a properly selected level of the external strain-rate also the stress level is very close to that obtained from the analytical model and presented in Figure 8B.

This has been confirmed numerically by using the explicit time integration scheme applied to the standard power-law rate-dependent regularization[78] of otherwise the same plasticity model of Cu single crystals,

$$\dot{\gamma}^{\alpha} = \begin{cases} \dot{\gamma}_0 \left(\frac{\tau^{\alpha}}{\tau_{\mathrm{c}}^{\alpha}} \right)^{\frac{1}{m}} & \text{if} \quad \tau^{\alpha} \geqslant 0, \\ 0 & \text{otherwise.} \end{cases} \tag{68}$$

Frequently used reference shear-rate $\dot{\gamma}_0 = 0.001 s^{-1}$ has been adopted.[73] A strain-rate-sensitivity parameter $m = 0.015$, typical at room temperature, has been taken to ensure convergence for an elongation step $\Delta\lambda = 10^{-5}$.

The stress level depends now on the elongation rate $\Delta\lambda/\Delta t$. It can be taken equal to $\Delta\lambda/\Delta t = 8\dot{\gamma}_0\lambda/\sqrt{6} \approx 0.004$ 1/s so that $\dot{\gamma}^{\alpha} \approx \dot{\gamma}_0$. An interesting conclusion obtained from formula (68) is that the stress level is then practically independent of the value of the rate-sensitivity parameter m. Since the elasticity effects are negligible, the analytical results shown in Figure 8B also represent the results calculated for the rate-dependent model, except for the initial elastic response which was missing from the rigid-plastic model. Unlike the stress-strain curve itself, the equal activity of eight equally stressed slip-systems is independent of material parameters, and the lattice orientation is represented by a single center point in Figure 8B contrary to the experiment. This is because the standard RD algorithm does not have a built-in mechanism of slip-system selection that could enforce a deviation from the initially imposed symmetry.

Uniaxial tension in the high symmetry orientation examined here can also be qualitatively compared with a number of results calculated in the literature using a rate-dependent model.[27,79,80] It is typical for RD models that from the outset of deformation the eight slip-systems become and remain active in this high-symmetry orientation. The results of RD models are thus qualitatively different from those obtained by applying QEP for the selection of active slip-systems and shown in Figure 8A.

We come back now to the simulations of simple shear presented in Section 5.1 and compare them to those based on the rate-dependent (RD) regularization with $m = 0.015$. Material parameters for both QEP and RD approaches are set as in Section 5.1, except the initial yield stress changed to $\tau_0 = 10$ MPa in order to avoid numerical instabilities in the RD simulations at the onset of plastic range. The difference in the initial value of yield stress has in fact a little effect on the stress-strain curves shown on a large-strain scale. The initial portions are different, but on this scale the difference is hardly visible. This is understandable because at large strain the initial stress level does not significantly affect the hardening behavior governed by the formula (64) with the same material parameters for QEP and RD.

Consider first the case of simple shear No. (3). The results of simple shear No. (3) generated by the QEP algorithm for the step size $\Delta\lambda = 0.01$ were previously shown in Figures 5 and 6. Calculations with the use of the RD regularization have been conducted for two shear rates, $\Delta\lambda/\Delta t = 1$/s and $\Delta\lambda/\Delta t = 0.002$ 1/s. In each case, a much smaller step size

$\Delta\lambda = 10^{-5}$ was used. A sufficient accuracy of RD calculations was confirmed by decreasing the step size to $\Delta\lambda = 10^{-6} = 1\ \Delta t$/s and obtaining practically the same results (not presented here) up to $\lambda = 1$.

The level of Kirchhoff stress τ_{13} calculated for $\Delta\lambda/\Delta t = 1$/s for the RD model is visibly higher than that determined by the QEP algorithm, Figure 9. However, the sets of active slip-systems and the predicted changes in the orientation of crystallographic axes are the same for the QEP and RD calculations, which results in the very similar shape of the corresponding stress curves. Finally, by reducing the shear rate to $\Delta\lambda/\Delta t = 0.002$ 1/s, the results for rate-independent (QEP) and rate-dependent (RD) calculations become undistinguishable in this particular case of simple shear as shown in Figure 9.

While for uniaxial tension in the high-symmetry direction the RD results corresponding to Figure 8B are hardly acceptable, in the above case of simple shear No. (3) the RD results can coincide with the QEP results. This is so because in the former case the criterion for selection of active slip-systems plays a crucial role while it is not needed in the latter example. In general, substantial differences between the QEP and RD results can be expected.

This is so in the case of simple shear No. (1), where the slip-system selection is again essential. Significant differences are visible in Figure 10 between the stress-strain curves obtained from the QEP algorithm and the rate-dependent (RD) model. Material parameters are again the same as in Section 5.1, except the initial yield stress set here to $\tau_0 = 10$ MPa. Calculations for the rate-dependent model (RD) have been performed using the previous parameters $m = 0.015$ and $\dot{\gamma}_0 = 0.001s^{-1}$, and step size $\Delta\lambda = 10^{-5} = 0.002\ \Delta t$/s until reaching $\lambda = 5$. The step size for QEP calculations was set much

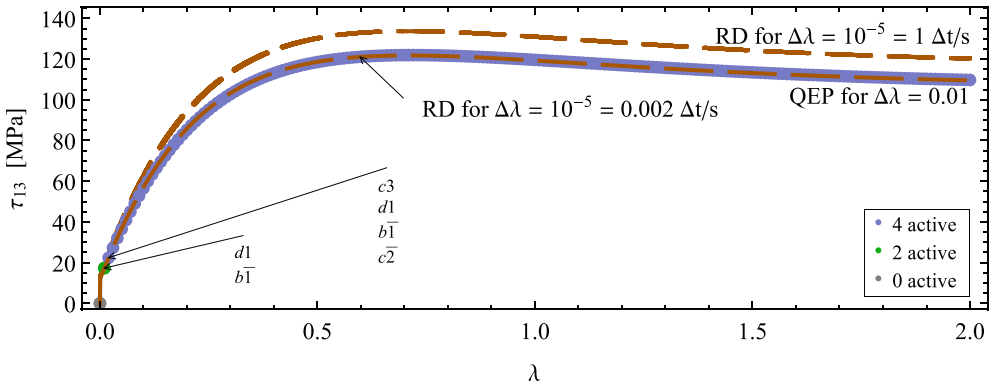

FIGURE 9 Simulations of simple shear No. (3). The QEP results (colored plot markers) are compared to rate-dependent (RD) simulations (broken lines) for shear increment $\Delta\lambda = 10^{-5}$ and two different time steps $\Delta t = 10^{-5}$ s and $\Delta t = 0.005$ s. Initial yield stress $\tau_0 = 10$ MPa, rate sensitivity parameter $m = 0.015$, reference shear-rate $\dot{\gamma}_0 = 0.001\text{s}^{-1}$

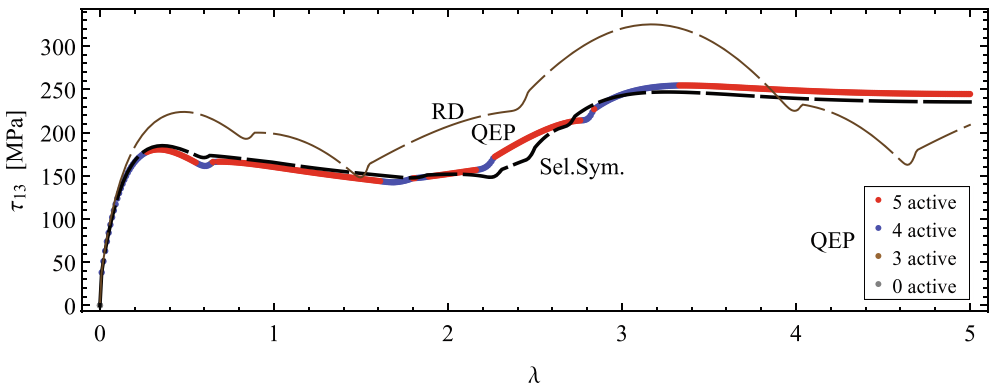

FIGURE 10 Simulations of simple shear No. (1). The QEP results (colored plot markers) are compared to those obtained for the selective symmetrization of $(g^{\alpha\beta})$ (dashed black line), both for shear increment $\Delta\lambda = 0.01$, and to rate-dependent (RD) simulations (broken brown line) for $\Delta\lambda = 10^{-5} = 0.002\ \Delta t$/s, $\dot{\gamma}_0 = 0.001s^{-1}$ and $m = 0.015$. Initial yield stress $\tau_0 = 10$ MPa

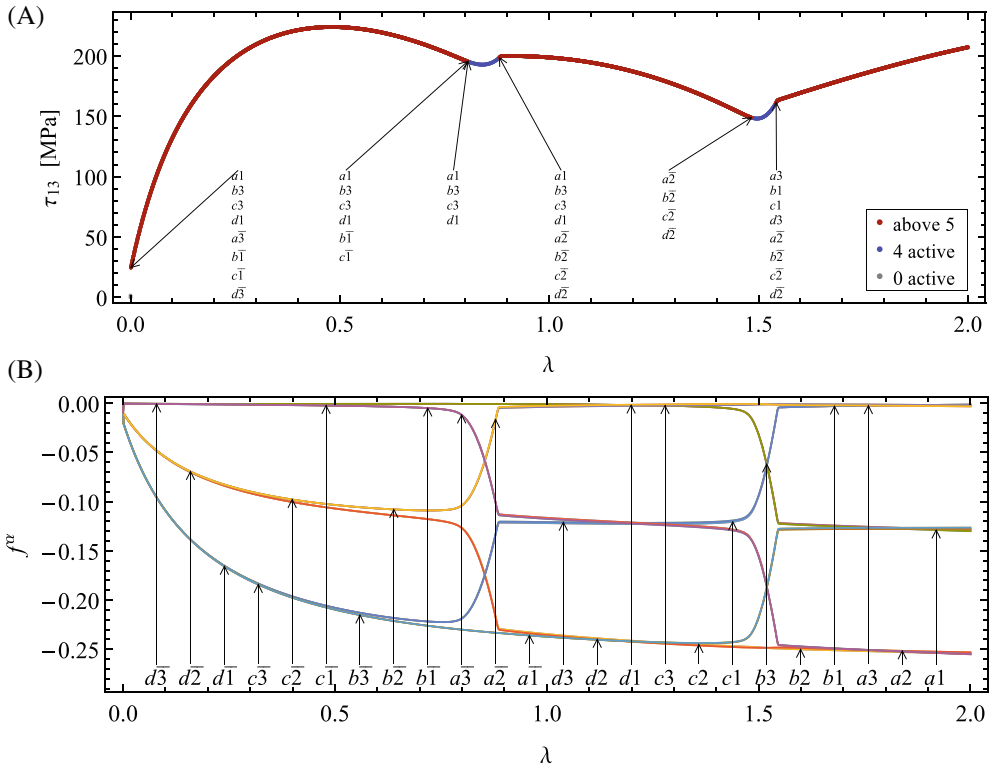

FIGURE 11 Rate-dependent simulation of simple shear No. (1): (A) shear stress τ_{13} versus shear strain with the active slip-system sets marked, and (B) corresponding values of the yield functions f^α for all slip systems, for $\Delta\lambda = 10^{-5} = 0.002\ \Delta t/\text{s}$, $\dot{\gamma}_0 = 0.001 s^{-1}$, $m = 0.015$, $\tau_0 = 10$ MPa

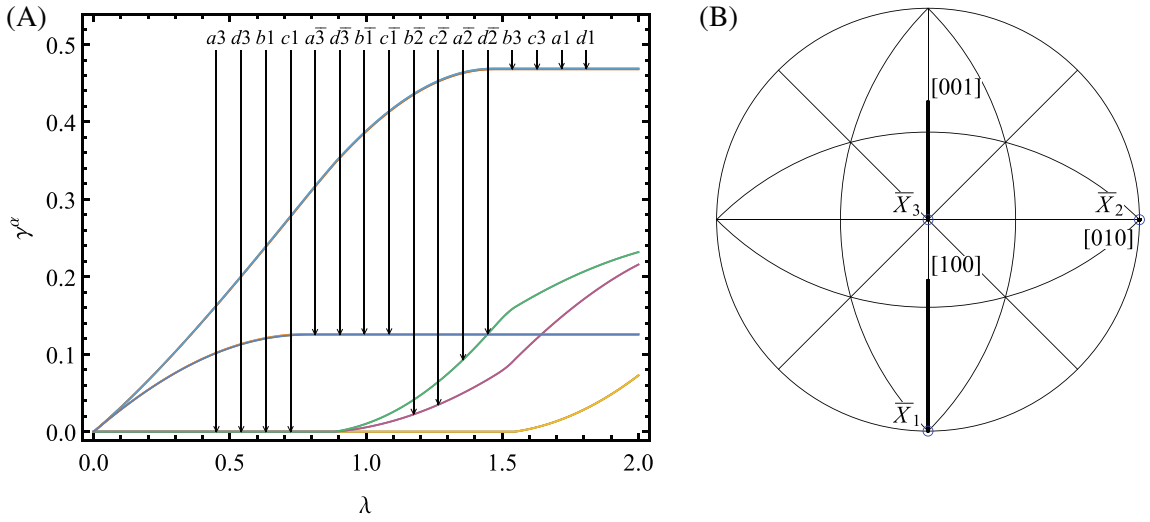

FIGURE 12 Rate-dependent simulation of simple shear No. (1): (A) accumulated slips on different systems and (B) changes in the orientation of crystallographic axes, for $\Delta\lambda = 10^{-5} = 0.002\ \Delta t/\text{s}$, $\dot{\gamma}_0 = 0.001 s^{-1}$, $m = 0.015$, $\tau_0 = 10$ MPa

larger, $\Delta\lambda = 10^{-2}$ as in the previous sections. In effect, the overall calculation time for the QEP algorithm was much shorter than that for the RD model.

The differences between the RD and QEP stress-strain curves in Figure 10 can be attributed to the difference in the predicted sets of active slip-systems. For many stages of deformation the rate-dependent model (RD) predicts activity of more than five slip-systems with $\Delta\gamma^\alpha > 0$, Figure 11. The difference in the prediction of lattice rotation is particularly striking, compare Figures 12B and 2B. It results from different sets of active slip systems, compare Figures 1, 2 and Figures 11, 12.

The results shown in Figure 10 are also compared with the calculations performed using the selective symmetrization[7] of the interaction moduli submatrix of $(g^{\alpha\beta})$ restricted to *active* slip-systems. The respective dashed black line differs somewhat from the QEP results obtained without that symmetrization. The difference is not substantial, which confirms that the selective symmetrization proposed in Reference 65 and applied in References 7 and 46 may be a good approximation.

Further work is in progress on nonunique deformation patterns calculated using the quasi-extremal energy principle.

6 | CONCLUSION

A constitutive algorithm for the rate-independent crystal plasticity has been proposed which enables automatic selection of active slip systems along large deformation paths using an energetic criterion. For the first time, this energy approach makes full use of the entire nonsymmetric slip-system interaction matrix, and not just its symmetrized part as in the incremental energy minimization approach. The algorithm is general enough to allow the inclusion of user-defined constitutive functions, such as hardening moduli $h^{\alpha\beta}$ specified in terms of any internal variables, or free energy density ϕ with its arbitrary split into elastic and plastic parts, to the constitutive standard framework derived from Reference 2.

The new key part of the algorithm is based on the recently proposed in Reference 1 quasi-extremal energy principle (QEP) applicable to nonpotential problems in rate-independent plasticity. To build it up, QEP is here extended to finite increments in the backward-Euler computational scheme for nonpotential problems of crystal plasticity. The other parts of the algorithm were adapted from the previous paper by the authors,[7] now with the extra term $\sum_{\alpha\beta} \tilde{\gamma}^\alpha g^{\alpha\beta}_{\text{skew}} \Delta\gamma^\beta$ added to a (generally nonconvex) incremental work expression. In this way, the incremental work minimization (limited to potential problems) has been extended to quasi-minimization of the energy expression for the nonpotential problems with nonsymmetric matrix $(g^{\alpha\beta})$. It has been shown that a solution to QEP formulated at a material point solves the local incremental problem so that all yield functions satisfy the discrete consistency conditions at the end of a time step. It is essential that the active slip-system set is obtained as part of the solution to the minimization problem for an augmented Lagrangian, in distinction to other approaches where the set is *assumed* before solving the system of incremental equations.

The effectiveness of the QEP algorithm has been illustrated by the numerical examples calculated for a fcc single crystal subjected to simple shear or uniaxial tension. It has been shown that the algorithm enables the *automatic* selection of a set of active slip-systems during the simulations. The obtained results differ significantly from those calculated using the rate-dependent modeling without any criterion of slip-system selection, see Figures 8 and 10. The comparison with the experimental data presented in Figure 8 shows that the QEP results in this case are much closer to the experimental test in terms of the number of active slip-systems and the rotation of the crystallographic lattice. The QEP modeling can therefore be more reliable in describing the actual plastic response of metal crystals than conventional rate-dependent modeling in cases where the selection of active slip-systems is essential.

In the outlook, an analogous QEP-based approach can be applied to other nonpotential inelastic problems as a generalization of the previous algorithms based on the incremental energy minimization approach with the automatic branch switching on deformation paths, see References 38,39,46.

ENDNOTE

Notation: Bold-face characters are used to denote vectors (in a three-dimensional Euclidean space) or second-order tensors, and doublestruck capitals (like $\mathbb{C}$) denote fourth-order tensors. Direct juxtaposition of two tensors means simple contraction, a central dot – double contraction in the sense $\mathbf{A} \cdot \mathbf{B} = A_{ij}B_{ij}$, and $\otimes$ a tensor product. A superimposed -1, T or $-$T over a tensor symbol denotes an inverse, transpose or transposed inverse, respectively. A superimposed dot denotes the rate, understood as the material time derivative in the one-sided (forward) sense, $\mathrm{d}/\mathrm{d}t^+$, which is assumed to exist. A Greek superscript denotes a slip-system index (not an exponent). Symbol $:=$ is used to distinguish a definition or substitution from an equality.

ORCID

Henryk Petryk https://orcid.org/0000-0003-3454-8325

REFERENCES

1. Petryk H. A quasi-extremal energy principle for non-potential problems in rate-independent plasticity. *J Mech Phys Solids*. 2020;136:103691.
2. Hill R, Rice JR. Constitutive analysis of elastic-plastic crystals at arbitrary strain. *J Mech Phys Solids*. 1972;20:401-413.
3. Peirce D, Asaro RJ, Needleman A. An analysis of nonuniform and localized deformation in ductile single crystals. *Acta Metall*. 1982;30(6):1087-1119.
4. Franciosi P, Zaoui A. Crystal hardening and the issue of uniqueness. *Int J Plast*. 1991;7:295-311.
5. Petryk H. General conditions for uniqueness in materials with multiple mechanisms of inelastic deformation. *J Mech Phys Solids*. 2000;48:367-396.
6. Ortiz M, Repetto EA, Stainier L. A theory of subgrain dislocation structures. *J Mech Phys Solids*. 2000;48:2077-2114.
7. Petryk H, Kursa M. Incremental work minimization algorithm for rate-independent plasticity of single crystals. *Int J Numer Methods Eng*. 2015;104(3):157-184.
8. Hill R. Generalized constitutive relations for incremental deformation of metal crystals by multislip. *J Mech Phys Solids*. 1966;14(2):95-102.
9. Rice JR. Inelastic constitutive relations for solids: an internal-variable theory and its application to metal plasticity. *J Mech Phys Solids*. 1971;19:433-455.
10. Asaro RJ. Micromechanics of crystals and polycrystals. *Adv Appl Mech*. 1983;23:1-115.
11. Havner KS. *Finite Plastic Deformation of Crystalline Solids*. Cambridge University Press; 1992.
12. Bassani JL. Plastic flow of crystals. *Adv Appl Mech*. 1994;30:191-258.
13. Bigoni D. *Nonlinear Solid Mechanics: Bifurcation Theory and Material Instability*. Cambridge University Press; 2012.
14. Hackl K, Fischer F, Svoboda J. On the treatment of non-reciprocal rate-independent kinetics via thermodynamic extremal principles. *J Mech Phys Solids*. 2020;145:104149.
15. Svendsen B, Bargmann S. On the continuum thermodynamic rate variational formulation of models for extended crystal plasticity at large deformation. *J Mech Phys Solids*. 2010;58(9):1253-1271.
16. Reddy B. Some theoretical and computational aspects of single-crystal strain-gradient plasticity. *ZAMM - J Appl Math Mech*. 2013;93(12):844-867.
17. Miehe C, Mauthe S, Hildebrand F. Variational gradient plasticity at finite strains. Part III: local-global updates and regularization techniques in multiplicative plasticity for single crystals. *Comput Methods Appl Mech Eng*. 2014;268:735-762.
18. Erdle H, Böhlke T. A gradient crystal plasticity theory for large deformations with a discontinuous accumulated plastic slip. *Comput Mech*. 2017;60:923-942.
19. Lewandowski M, Stupkiewicz S. Size effects in wedge indentation predicted by a gradient-enhanced crystal-plasticity model. *Int J Plast*. 2018;109:54-78.
20. Po G, Huang Y, Ghoniem N. A continuum dislocation-based model of wedge microindentation of single crystals. *Int J Plast*. 2019;114:72-86.
21. Dequiedt J. Selection of slip systems in confined single crystal gradient plasticity: coupled effects of slip system orientations, latent hardening, and grain boundaries. *Arch Mech*. 2019;71(3):207-238.
22. Reddy B, Steinmann P, Kergaßner A. A thermodynamically consistent theory of stress-gradient plasticity. *J Mech Phys Solids*. 2021;147:104266.
23. de Souza Neto EA, Perić D, Owen DRJ. *Computational Methods for Plasticity: Theory and Applications*. John Wiley & Sons, Ltd; 2008.
24. Simo JC, Kennedy JG, Govindjee S. Non-smooth multisurface plasticity and viscoplasticity. Loading/unloading conditions and numerical algorithms. *Int J Numer Methods Eng*. 1988;26(10):2161-2185.
25. Simo JC, Hughes TJR. *Computational inelasticity. Interdisciplinary Applied Mathematics*. Vol 7. Springer-Verlag; 1998.
26. Borja RI, Wren JR. Discrete micromechanics of elastoplastic crystals. *Int J Numer Methods Eng*. 1993;36(22):3815-3840.
27. Anand L, Kothari M. A computational procedure for rate-independent crystal plasticity. *J Mech Phys Solids*. 1996;44(4):525-558.
28. Miehe C. Multisurface thermoplasticity for single crystals at large strains in terms of Eulerian vector updates. *Int J Solids Struct*. 1996;33(20-22):3103-3130.
29. Schmidt-Baldassari M. Numerical concepts for rate-independent single crystal plasticity. *Comput Methods Appl Mech Eng*. 2003;192(11-12):1261-1280.
30. Schröder J, Miehe C. Aspects of computational rate-independent crystal plasticity. *Comput Mater Sci*. 1997;9(1-2):168-176.
31. Busso EP, Cailletaud G. On the selection of active slip systems in crystal plasticity. *Int J Plast*. 2005;21(11):2212-2231.
32. McGinty RD, McDowell DL. A semi-implicit integration scheme for rate independent finite crystal plasticity. *Int J Plast*. 2006;22(6):996-1025.
33. Ben Bettaieb M, Débordes O, Dogui A, Duchêne L, Keller C. On the numerical integration of rate independent single crystal behavior at large strain. *Int J Plast*. 2012;32-33:184-217.
34. Forest S, Rubin M. A rate-independent crystal plasticity model with a smooth elastic-plastic transition and no slip indeterminacy. *Eur J Mech A/Solids*. 2016;55:278-288.
35. Prüger S, Kiefer B. A comparative study of integration algorithms for finite single crystal (visco-)plasticity. *Int J Mech Sci*. 2020;180:105740.
36. Scheunemann L, Nigro P, Schröder J, Pimenta P. A novel algorithm for rate independent small strain crystal plasticity based on the infeasible primal-dual interior point method. *Int J Plast*. 2020;124:1-19.
37. Zhang M, Nguyen K, Segurado J, Montáns FJ. A multiplicative finite strain crystal plasticity formulation based on additive elastic corrector rates: theory and numerical implementation. *Int J Plast*. 2021;137:102899.

38. Petryk H, Thermann K. On discretized plasticity problems with bifurcations. *Int J Solids Struct*. 1992;29(6):745-765.
39. Petryk H, Thermann K. Post-critical plastic deformation in incrementally nonlinear materials. *J Mech Phys Solids*. 2002;50:925-954.
40. Carstensen C, Hackl K, Mielke A. Non-convex potentials and microstructures in finite-strain plasticity. *Proc R Soc Lond A*. 2002;458:299-317.
41. Mielke A. Energetic formulation of multiplicative elasto-plasticity using dissipation distances. *Contin Mech Thermodyn*. 2003;15(4):351-382.
42. Miehe C, Lambrecht M, Gürses E. Analysis of material instabilities in inelastic solids by incremental energy minimization and relaxation methods: evolving deformation microstructures in finite plasticity. *J Mech Phys Solids*. 2004;52:2725-2769.
43. Kratochvíl J, Kružík M, Sedláček R. Instability origin of subgrain formation in plastically deformed materials. *Int J Eng Sci*. 2010;48:1401-1412.
44. Kochmann DM, Hackl K. The evolution of laminates in finite crystal plasticity: a variational approach. *Contin Mech Thermodyn*. 2011;23:63-85.
45. Homayonifar M, Mosler J. Efficient modeling of microstructure evolution in magnesium by energy minimization. *Int J Plast*. 2012;28(1):1-20.
46. Petryk H, Kursa M. The energy criterion for deformation banding in ductile single crystals. *J Mech Phys Solids*. 2013;61(8):1854-1875.
47. Kumar S, Vidyasagar A, Kochmann DM. An assessment of numerical techniques to find energy-minimizing microstructures associated with nonconvex potentials. *Int J Numer Methods Eng*. 2020;121(7):1595-1628.
48. Peirce D, Asaro RJ, Needleman A. Material rate dependence and localized deformation in crystalline solids. *Acta Metall*. 1983;31(12):1951-1976.
49. Cuitiño AM, Ortiz M. Computational modelling of single crystals. *Model Simul Mater Sci Eng*. 1993;1(3):225-263.
50. Lebensohn R, Tomé C. A self-consistent anisotropic approach for the simulation of plastic deformation and texture development of polycrystals: application to zirconium alloys. *Acta Metall Mater*. 1993;41(9):2611-2624.
51. Anand L, Kalidindi SR. The process of shear band formation in plane strain compression of FCC metals: effects of crystallographic texture. *Mech Mater*. 1994;17(2-3):223-243.
52. Raabe D, Roters F. Using texture components in crystal plasticity finite element simulations. *Int J Plast*. 2004;20(3):339-361.
53. Dequiedt J. The incidence of slip system interactions on the deformation of FCC single crystals: system selection and segregation for local and non-local constitutive behavior. *Int J Solids Struct*. 2018;141-142:1-14.
54. Ortiz M, Stainier L. The variational formulation of viscoplastic constitutive updates. *Comput Methods Appl Mech Eng*. 1999;171(3-4):419-444.
55. Homayonifar M, Mosler J. On the coupling of plastic slip and deformation-induced twinning in magnesium: a variationally consistent approach based on energy minimization. *Int J Plast*. 2011;27(7):983-1003.
56. Bargmann S, Svendsen B, Ekh M. An extended crystal plasticity model for latent hardening in polycrystals. *Comput Mech*. 2011;48(6):631-645.
57. Yalcinkaya T, Brekelmans W, Geers M. Deformation patterning driven by rate dependent non-convex strain gradient plasticity. *J Mech Phys Solids*. 2011;59(1):1-17.
58. Hill R. Aspects of invariance in solids mechanics. *Adv Appl Mech*. 1978;18:1-75.
59. Asaro RJ, Rice JR. Strain localization in ductile single crystals. *J Mech Phys Solids*. 1977;25(5):309-338.
60. Hill R. A theory of the yielding and plastic flow of anisotropic metals. *Proc R Soc Lond A*. 1948;193(1033):281-297.
61. Bishop JFW, Hill R. A theory of the plastic distortion of a polycrystalline aggregate under combined stresses. *Philos Mag*. 1951;42(327):414-427.
62. Petryk H. Thermodynamic conditions for stability in materials with rate-independent dissipation. *Philos Trans R Soc Lond A*. 2005;363:2479-2515.
63. Kröner E. Allgemeine kontinuumstheorie der versetzungen und eigenspannungen. *Arch Ration Mech Anal*. 1960;4(1):273-334.
64. Mandel J. *Plasticité classique et viscoplasticité, CISM Courses and Lectures*. Vol 97. Springer-Verlag; 1971.
65. Petryk H, Kursa M. Selective symmetrization of the slip-system interaction matrix in crystal plasticity. *Arch Mech*. 2011;63(3):287-310.
66. Petryk H. Incremental energy minimization in dissipative solids. *C R Mecanique*. 2003;331:469-474.
67. Petryk H. A consistent energy approach to defining stability of plastic deformation processes. In: Schroeder FH, ed. *IUTAM Symposium on Stability in the mechanics of continua, Nümbrecht 1981*. Springer; 1982:262-272.
68. Miehe C. Exponiential map algorithm for stress updates in anisotropic multiplicative elastoplasticity for single crystals. *Int J Numer Methods Eng*. 1996;39(19):3367-3390.
69. Steinmann P, Stein E. On the numerical treatment and analysis of finite deformation ductile single crystal plasticity. *Comput Methods Appl Mech Eng*. 1996;129(3):235-254.
70. Bertsekas DP. *Constrained Optimization and Lagrange Multiplier Methods*. 2nd ed. Athena Scientific; 1996.
71. Nocedal J, Wright SJ. *Numerical Optimization*. Springer-Verlag; 1999.
72. Taylor GI. Analysis of plastic strain in a cubic crystal. In: Lessels JM, ed. *Stephen Timoshenko 60th Anniversary*. Macmillan; 1938: 218-224.
73. Bronkhorst CA, Kalidindi SR, Anand L. Polycrystalline plasticity and the evolution of crystallographic texture in FCC metals. *Philos Trans R Soc Lond A*. 1992;341(1662):443-477.
74. Kucharski S, Woźniacka S. Size effect in single crystal copper examined with spherical indenters. *Metall Mater Trans A*. 2019;50:2139-2154.
75. Simmons G, Wang H. *Single Crystal Elastic Constants and Calculated Aggregate Properties: A Handbook*. 2nd ed. MIT Press; 1971.

76. Bertram A, Kraska M. Description of finite plastic deformations in single crystals by material isomorphisms. In: Parker DF, England AH, eds. *IUTAM Symposium on Anisotropy, Inhomogeneity and Nonlinearity in Solid Mechanics*. Springer; 1995:77-90.
77. Saeki Y, Miura S. Plastic deformation and prominent cross slip of ⟨100⟩ oriented aluminum single crystals. *Trans Jpn Inst Met*. 1977;18:843-851.
78. Hutchinson JW. Bounds and self-consistent estimates for creep of polycrystalline materials. *Proc R Soc Lond A*. 1976;348(1652):101-127.
79. Staroselsky A, Cassenti BN. Combined rate-independent plasticity and creep model for single crystal. *Mech Mater*. 2010;42(10):945-959.
80. Zamiri AR, Pourboghrat F. A novel yield function for single crystals based on combined constraints optimization. *Int J Plast*. 2010;26(5):731-746.

How to cite this article: Petryk H, Kursa M. Crystal plasticity algorithm based on the quasi-extremal energy principle. *Int J Numer Methods Eng*. 2022;123(14):3285-3316. doi: 10.1002/nme.6969

APPENDIX . DERIVATION OF THE ENERGY EXPRESSION FOR THE INCREMENTAL PROBLEM

The expression for a finite increment of the internal work density for an arbitrary history of virtual *rates* $(\tilde{\mathbf{F}}_t, \tilde{\gamma}^\alpha_t) := (\tilde{\mathbf{F}}(t), \tilde{\gamma}^\alpha(t))$, at constant coefficients $(\mathbb{C}^{\mathrm{e}}, \mathbf{\Lambda}^\alpha, g^{\alpha\beta})$ of constitutive rate-equations (16) with $\mathbb{C}^{\mathrm{e}} = \overset{\mathrm{T}}{\mathbb{C}}{}^{\mathrm{e}}$ and $(g^{\alpha\beta})$ an arbitrarily nonsymmetric matrix, is obtained by *backward* time integration of the virtual work rate (6) as follows

$$
\begin{aligned}
\Delta w :&= \int_{t_n}^{t_{n+1}} \left(\left(\mathbf{S}_{n+1} - \int_t^{t_{n+1}} \tilde{\mathbf{S}}(\theta)\mathrm{d}\theta \right) \cdot \tilde{\mathbf{F}}_t - \sum_{\alpha\in\mathcal{N}} \left(f^\alpha_{n+1} - \int_t^{t_{n+1}} \tilde{f}^\alpha(\theta)\mathrm{d}\theta \right) \tilde{\gamma}^\alpha_t \right) \mathrm{d}t \\
&= \mathbf{S}_{n+1}\cdot\Delta\mathbf{F} - \sum_{\alpha\in\mathcal{N}} f^\alpha_{n+1}\Delta\gamma^\alpha - \int_{t_n}^{t_{n+1}} \left(\int_t^{t_{n+1}} \left(\mathbb{C}^{\mathrm{e}}\cdot\tilde{\mathbf{F}}(\theta) - \sum_{\alpha\in\mathcal{N}} \mathbf{\Lambda}_\alpha \tilde{\gamma}^\alpha(\theta) \right) \mathrm{d}\theta \right) \cdot \tilde{\mathbf{F}}_t \mathrm{d}t \\
&\quad + \int_{t_n}^{t_{n+1}} \sum_{\alpha\in\mathcal{N}} \left(\int_t^{t_{n+1}} \left(\tilde{\mathbf{F}}(\theta)\cdot\mathbf{\Lambda}_\alpha - \sum_{\beta\in\mathcal{N}} g^{\alpha\beta}\tilde{\gamma}^\beta(\theta) \right) \mathrm{d}\theta\tilde{\gamma}^\alpha_t \right) \mathrm{d}t \\
&= \mathbf{S}_{n+1}\cdot\Delta\mathbf{F} - \sum_{\alpha\in\mathcal{N}} f^\alpha_{n+1}\Delta\gamma^\alpha - \int_{t_n}^{t_{n+1}} \left(\mathbb{C}^{\mathrm{e}}\cdot(\mathbf{F}_{n+1}-\mathbf{F}_t) - \sum_{\alpha\in\mathcal{N}} \mathbf{\Lambda}_\alpha(\gamma^\alpha_{n+1}-\gamma^\alpha_t) \right) \cdot \tilde{\mathbf{F}}_t \mathrm{d}t \\
&\quad + \int_{t_n}^{t_{n+1}} \sum_{\alpha\in\mathcal{N}} \left((\mathbf{F}_{n+1}-\mathbf{F}_t)\cdot\mathbf{\Lambda}_\alpha - \sum_{\beta\in\mathcal{N}} g_{\alpha\beta}(\gamma^\beta_{n+1}-\gamma^\beta_t) \right) \tilde{\gamma}^\alpha_t \mathrm{d}t \\
&= \mathbf{S}_{n+1}\cdot\Delta\mathbf{F} - \sum_{\alpha\in\mathcal{N}} f^\alpha_{n+1}\Delta\gamma^\alpha + \int_{t_n}^{t_{n+1}} \frac{\mathrm{d}}{\mathrm{d}t} \left((\mathbf{F}_{n+1}-\mathbf{F}_t)\cdot\left(\frac{1}{2}\mathbb{C}^{\mathrm{e}}\cdot(\mathbf{F}_{n+1}-\mathbf{F}_t) - \sum_{\alpha\in\mathcal{N}} \mathbf{\Lambda}_\alpha(\gamma^\alpha_{n+1}-\gamma^\alpha_t) \right) \right) \mathrm{d}t \\
&\quad + \sum_{\alpha,\beta\in\mathcal{N}} \left(\int_{t_n}^{t_{n+1}} \frac{1}{2} g_{\alpha\beta} \frac{\mathrm{d}}{\mathrm{d}t} \left((\gamma^\beta_{n+1}-\gamma^\beta_t)(\gamma^\alpha_{n+1}-\gamma^\alpha_t) \right) \mathrm{d}t - \int_{t_n}^{t_{n+1}} \frac{1}{2} g_{\alpha\beta} \left((\gamma^\beta_{n+1}-\gamma^\beta_t)\tilde{\gamma}^\alpha_t + \tilde{\gamma}^\beta_t(\gamma^\alpha_{n+1}-\gamma^\alpha_t) \right) \mathrm{d}t \right) \\
&= \mathbf{S}_{n+1}\cdot\Delta\mathbf{F} - \frac{1}{2}\Delta\mathbf{F}\cdot\mathbb{C}^{\mathrm{e}}\cdot\Delta\mathbf{F} - \sum_{\alpha\in\mathcal{N}} \left(f^\alpha_{n+1} - \mathbf{\Lambda}^\alpha\cdot\Delta\mathbf{F} \right) \Delta\gamma^\alpha - \frac{1}{2}\sum_{\alpha,\beta\in\mathcal{N}} \Delta\gamma^\alpha g^{\alpha\beta}\ \Delta\gamma^\beta \\
&\quad - \frac{1}{2}\sum_{\alpha,\beta\in\mathcal{N}} \int_{t_n}^{t_{n+1}} \tilde{\gamma}^\alpha_t (g^{\alpha\beta} - g^{\beta\alpha})\ (\gamma^\beta_{n+1}-\gamma^\beta_t)\mathrm{d}t,
\end{aligned}
\tag{A1}
$$

where

$$
\Delta\mathbf{F} := \int_{t_n}^{t_{n+1}} \tilde{\mathbf{F}}_t\ \mathrm{d}t \geq 0, \quad \Delta\gamma^\alpha := \int_{t_n}^{t_{n+1}} \tilde{\gamma}^\alpha_t\ \mathrm{d}t \geq 0, \quad \gamma^\beta_t := \int_{t_n}^{t} \tilde{\gamma}^\beta_\theta\ \mathrm{d}\theta. \tag{A2}
$$

For constant coefficients $\mathbb{C}^{\mathrm{e}} = \overset{\mathrm{T}}{\mathbb{C}}{}^{\mathrm{e}}$, $\mathbf{\Lambda}^{\alpha}$, and $g^{\alpha\beta}$, the work expression (A1) is *exact*. Under the same assumptions, the immediate consequence of the constitutive rate Equation (16) is that the quantities

$$\hat{\Delta}\mathbf{S} := \mathbb{C}^{\mathrm{e}} \cdot \Delta\mathbf{F} - \sum_{\alpha\in\mathcal{N}} \mathbf{\Lambda}_{\alpha}\Delta\gamma^{\alpha}, \quad \hat{\Delta}f^{\alpha} := \Delta\mathbf{F}\cdot\mathbf{\Lambda}_{\alpha} - \sum_{\beta\in\mathcal{N}} g_{\alpha\beta}\Delta\gamma^{\beta} \tag{A3}$$

satisfy the equalities

$$\mathbf{S}_{n+1} = \mathbf{S}_n + \hat{\Delta}\mathbf{S}, \qquad f^{\alpha}_{n+1} = f^{\alpha}_n + \hat{\Delta}f^{\alpha} \quad \text{for constant } \mathbb{C}^{\mathrm{e}}, \mathbf{\Lambda}^{\alpha}, g^{\alpha\beta}. \tag{A4}$$

Jointly with the identity $\sum_{\alpha,\beta\in\mathcal{N}} \Delta\gamma^{\alpha}(g^{\alpha\beta} - g^{\beta\alpha})\ \Delta\gamma^{\beta} = 0$, which implies

$$-\sum_{\alpha,\beta\in\mathcal{N}}\int_{t_n}^{t_{n+1}} \tilde{\gamma}^{\alpha}(t)(g^{\alpha\beta} - g^{\beta\alpha})\ (\gamma^{\beta}_{n+1} - \gamma^{\beta}_{t})\mathrm{d}t = \sum_{\alpha,\beta\in\mathcal{N}}\int_{t_n}^{t_{n+1}} \tilde{\gamma}^{\alpha}(t)(g^{\alpha\beta} - g^{\beta\alpha})\ (\gamma^{\beta}_{t} - \gamma^{\beta}_{n})\mathrm{d}t, \tag{A5}$$

this shows that the formula (A1) is equivalent to another exact formula given in Reference 7(Eq. (39)) under the assumption of *constant* coefficients. However, the coefficients are typically state-dependent and vary continuously along a straining path, and then the equivalence no longer holds. The final formula (A1) with

$$\mathbb{C}^{\mathrm{e}} := \mathbb{C}^{\mathrm{e}}_{n+1}, \quad \mathbf{\Lambda}^{\alpha} := \mathbf{\Lambda}^{\alpha}_{n+1}, \quad g^{\alpha\beta} := g^{\alpha\beta}_{n+1} \tag{A6}$$

is to be preferred when using the *implicit* Euler method. As shown in Section 4.1, this provides a natural derivation of the algorithmic refinement 1 postulated in Reference 7.

From formula (A1) it is clear that Δw depends on the final increment $\Delta\mathbf{F}$ regardless of the history of its rate $\dot{\mathbf{F}}(t)$, on account of $\mathbb{C}^{\mathrm{e}} = \overset{\mathrm{T}}{\mathbb{C}}{}^{\mathrm{e}}$. However, Δw depends not only on $\Delta\gamma^{\alpha}$ but is also a functional of the history of virtual slip-rates $\tilde{\gamma}^{\alpha}(t)$ in interval $[t_n, t_{n+1}]$, unless $(g^{\alpha\beta})$ is a symmetric matrix when restricted to $\alpha, \beta \in \mathcal{A} := \{\alpha \mid \Delta\gamma^{\alpha} > 0\}$.

Examine now a *strong* variation of the functional in the final expression (A1), taken relative to a solution path $\dot{\gamma}^{\alpha}(t) = \dot{\gamma}^{\alpha}_0 = \Delta\gamma^{\alpha}_0/(t_{n+1} - t_n) = \text{const} \geq 0$ in interval $[t_n, t_{n+1}]$. For this purpose, suppose that $\tilde{\gamma}^{\alpha}(t) = \dot{\gamma}^{\alpha}_0/\theta = \text{const}$ for $t \in [t_n, \tau]$, where $\tau - t_n = \theta(t_{n+1} - t_n)$ and $1 > \theta \approx 1$, so that the integral in Equation (A1) vanishes if restricted to the predominant subinterval $[t_n, \tau]$. Over the complementary small subinterval $[\tau, t_{n+1}]$, let the virtual rate $\tilde{\gamma}^{\alpha}(t)$ take another, arbitrarily different from $\dot{\gamma}^{\alpha}_0$ but constant value $\tilde{\gamma}^{\alpha}(t) = \tilde{\gamma}^{\alpha} = \text{const}$. Then $(\gamma^{\beta}_t - \gamma^{\beta}_n)$ is proportional to $\dot{\gamma}^{\beta}$ for $t \in [t_n, \tau]$, while $(\gamma^{\beta}_t - \gamma^{\beta}_{\tau})$ is proportional to $\tilde{\gamma}^{\beta}$ for $t \in [\tau, t_{n+1}]$, and $\Delta\gamma^{\alpha} = \Delta\gamma^{\alpha}_0 + (t_{n+1} - \tau)\tilde{\gamma}^{\alpha}$. Hence, the integral in Equation (A5) reduces successively to

$$\begin{aligned}
-\sum_{\alpha,\beta\in\mathcal{N}}\int_{t_n}^{t_{n+1}} \tilde{\gamma}^{\alpha}(t)(g^{\alpha\beta} - g^{\beta\alpha})\ (\gamma^{\beta}_{n+1} - \gamma^{\beta}_{t})\mathrm{d}t &= \sum_{\alpha,\beta\in\mathcal{N}}\int_{\tau}^{t_{n+1}} \tilde{\gamma}^{\alpha}(g^{\alpha\beta} - g^{\beta\alpha})\ (\gamma^{\beta}_{t} - \gamma^{\beta}_{n})\mathrm{d}t \\
&= \sum_{\alpha,\beta\in\mathcal{N}}\int_{\tau}^{t_{n+1}} \tilde{\gamma}^{\alpha}(g^{\alpha\beta} - g^{\beta\alpha})\ (\gamma^{\beta}_{t} - \gamma^{\beta}_{\tau} + \Delta\gamma^{\beta}_0)\mathrm{d}t \\
&= \sum_{\alpha,\beta\in\mathcal{N}} (t_{n+1} - \tau)\tilde{\gamma}^{\alpha}(g^{\alpha\beta} - g^{\beta\alpha})\Delta\gamma^{\beta}_0 \\
&= \sum_{\alpha,\beta\in\mathcal{N}} (\Delta\gamma^{\alpha} - \Delta\gamma^{\alpha}_0)(g^{\alpha\beta} - g^{\beta\alpha})\Delta\gamma^{\beta}_0 \\
&= \sum_{\alpha,\beta\in\mathcal{N}} \Delta\gamma^{\alpha}(g^{\alpha\beta} - g^{\beta\alpha})\Delta\gamma^{\beta}_0.
\end{aligned} \tag{A7}$$

Alternatively, to examine again a *strong* variation of functional (A1) but in a somewhat different way, suppose that $\tilde{\gamma}^{\alpha}(t) = \dot{\gamma}^{\alpha}_0 = \Delta\gamma^{\alpha}_0/(t_{n+1} - t_n) = \text{const}$ for $t \in [t_n, \tau]$ with $\tau - t_n = \theta(t_{n+1} - t_n)$, while $\tilde{\gamma}^{\alpha}(t)$ takes another constant value $\tilde{\gamma}^{\alpha}(t) = \hat{\gamma}^{\alpha} + \dot{\gamma}^{\alpha}_0 = \text{const}$ in the complementary subinterval $[\tau, t_{n+1}]$. Then $(\gamma^{\beta}_t - \gamma^{\beta}_n)$ is proportional to $\dot{\gamma}^{\beta}_0$ for $t \in [t_n, \tau]$, while $(\gamma^{\beta}_t - \gamma^{\beta}_{\tau})$ is proportional to $\hat{\gamma}^{\beta} + \dot{\gamma}^{\beta}_0$ for $t \in [\tau, t_{n+1}]$, and $\Delta\gamma^{\alpha} = \Delta\gamma^{\alpha}_0 + (t_{n+1} - \tau)\hat{\gamma}^{\alpha}$. Integral (A5) reduces now successively to

$$
\begin{aligned}
-\sum_{\alpha,\beta\in\mathcal{N}}\int_{t_n}^{t_{n+1}}\tilde{\gamma}^{\alpha}(t)(g^{\alpha\beta}-g^{\beta\alpha})\,(\gamma_{n+1}^{\beta}-\gamma_t^{\beta})\mathrm{d}t &= \sum_{\alpha,\beta\in\mathcal{N}}\int_{\tau}^{t_{n+1}}(\hat{\gamma}^{\alpha}+\dot{\gamma}_0^{\alpha})(g^{\alpha\beta}-g^{\beta\alpha})\,(\gamma_t^{\beta}-\gamma_n^{\beta})\mathrm{d}t\\
&= \sum_{\alpha,\beta\in\mathcal{N}}\int_{\tau}^{t_{n+1}}(\hat{\gamma}^{\alpha}+\dot{\gamma}_0^{\alpha})(g^{\alpha\beta}-g^{\beta\alpha})\,(\gamma_{\tau}^{\beta}-\gamma_n^{\beta})\mathrm{d}t\\
&= \sum_{\alpha,\beta\in\mathcal{N}}(t_{n+1}-\tau)(\hat{\gamma}^{\alpha}+\dot{\gamma}_0^{\alpha})(g^{\alpha\beta}-g^{\beta\alpha})(\gamma_{\tau}^{\beta}-\gamma_n^{\beta})\\
&= \sum_{\alpha,\beta\in\mathcal{N}}(\Delta\gamma^{\alpha}-\Delta\gamma_0^{\alpha})(g^{\alpha\beta}-g^{\beta\alpha})\theta\Delta\gamma_0^{\beta}\\
&= \theta\sum_{\alpha,\beta\in\mathcal{N}}\Delta\gamma^{\alpha}(g^{\alpha\beta}-g^{\beta\alpha})\Delta\gamma_0^{\beta}
\end{aligned}
\tag{A8}
$$

In the limit as $\theta\to 1$ we retrieve the final formula in Equation (A7), although this time with the relaxed restriction $\hat{\gamma}^{\alpha}+\dot{\gamma}_0^{\alpha}\geq 0$ (which implies $\Delta\gamma^{\alpha}\geq 0$) in place of previous $\tilde{\gamma}^{\alpha}\geq 0$ (which implied $\Delta\gamma^{\alpha}\geq\Delta\gamma_0^{\alpha}$). In either case, we arrive at the expression, denoted by $\Delta\varepsilon$, for Δw evaluated along the bi-linear path of γ_t^{α} as examined above, in the form

$$
\begin{aligned}
\Delta\varepsilon = \mathbf{S}_{n+1}\cdot\Delta\mathbf{F}-\frac{1}{2}\Delta\mathbf{F}\cdot\mathbb{C}^{\mathrm{e}}\cdot\Delta\mathbf{F}-\sum_{\alpha\in\mathcal{N}}\left(f_{n+1}^{\alpha}-\boldsymbol{\Lambda}^{\alpha}\cdot\Delta\mathbf{F}\right)\Delta\gamma^{\alpha}-\frac{1}{2}\sum_{\alpha,\beta\in\mathcal{N}}\Delta\gamma^{\alpha}g^{\alpha\beta}\,\Delta\gamma^{\beta}\\
+\sum_{\alpha,\beta\in\mathcal{N}}\Delta\gamma^{\alpha}g_{\mathrm{skew}}^{\alpha\beta}\Delta\gamma_0^{\beta},\qquad\text{where }\ g_{\mathrm{skew}}^{\alpha\beta}=\frac{1}{2}(g^{\alpha\beta}-g^{\beta\alpha}),
\end{aligned}
\tag{A9}
$$

for constant but arbitrary coefficients $\mathbb{C}^{\mathrm{e}}=\overset{\mathrm{T}}{\mathbb{C}^{\mathrm{e}}}$, $\boldsymbol{\Lambda}^{\alpha}$, and $g^{\alpha\beta}$. For a single linear path of any γ_t^{α} varying proportionally with time, the last term vanishes and $\Delta\varepsilon$ reduces to

$$
\overline{\Delta w}=\mathbf{S}_{n+1}\cdot\Delta\mathbf{F}-\sum_{\alpha\in\mathcal{N}}f_{n+1}^{\alpha}\Delta\gamma^{\alpha}-\Delta_2 w,
\tag{A10}
$$

where

$$
\begin{aligned}
\Delta_2 w &= \frac{1}{2}\Delta\mathbf{F}\cdot\mathbb{C}^{\mathrm{e}}\cdot\Delta\mathbf{F}-\sum_{\alpha\in\mathcal{N}}\left(\boldsymbol{\Lambda}^{\alpha}\cdot\Delta\mathbf{F}\right)\Delta\gamma^{\alpha}+\frac{1}{2}\sum_{\alpha,\beta\in\mathcal{N}}\Delta\gamma^{\alpha}g^{\alpha\beta}\,\Delta\gamma^{\beta}\\
&= \frac{1}{2}\hat{\Delta}\mathbf{S}\cdot\Delta\mathbf{F}-\frac{1}{2}\sum_{\alpha\in\mathcal{N}}\hat{\Delta}f^{\alpha}\Delta\gamma^{\alpha}\qquad\text{for constant }\ \mathbb{C}^{\mathrm{e}},\boldsymbol{\Lambda}^{\alpha},g^{\alpha\beta}.
\end{aligned}
\tag{A11}
$$